Award Number: W81XWH-17-1-0261

TITLE: A Novel Therapeutic Strategy Targeting BACH1 for Triple-Negative Breast Cancer

PRINCIPAL INVESTIGATOR: Jiyoung Lee

CONTRACTING ORGANIZATION: University of Chicago
Chicago, IL 60637

REPORT DATE: July 2019

TYPE OF REPORT: Annual

PREPARED FOR: U.S. Army Medical Research and Materiel Command
Fort Detrick, Maryland 21702-5012

REPORT DOCUMENTATION PAGE

Form Approved
OMB No. 0704-0188

1. REPORT DATE	2. REPORT TYPE	3. DATES COVERED
JULY 2019	Annual	1 JULY 2018 – 30 JUNE 2019

4. TITLE AND SUBTITLE

A Novel Therapeutic Strategy targeting BACH1 for Triple-Negative Breast Cancer

5a. CONTRACT NUMBER
W81XWH-17-1-0261

5b. GRANT NUMBER
1710261

5c. PROGRAM ELEMENT NUMBER

6. AUTHOR(S)

Jiyoung Lee

E-Mail: jlee218@uchicago.edu

5d. PROJECT NUMBER

5e. TASK NUMBER

5f. WORK UNIT NUMBER

7. PERFORMING ORGANIZATION NAME(S) AND ADDRESS(ES)

The University of Chicago
Ben May Department for Cancer Research
929 E. 57th street
Chicago, IL 60637

8. PERFORMING ORGANIZATION REPORT NUMBER

9. SPONSORING / MONITORING AGENCY NAME(S) AND ADDRESS(ES)
U.S. Army Medical Research and Materiel Command
Fort Detrick, Maryland 21702-5012

10. SPONSOR/MONITOR'S ACRONYM(S)

11. SPONSOR/MONITOR'S REPORT NUMBER(S)

12. DISTRIBUTION / AVAILABILITY STATEMENT
Approved for Public Release; Distribution Unlimited

13. SUPPLEMENTARY NOTES

14. ABSTRACT

Breast cancer is the second most cancer among women with a chance of 15% in their life time. The most aggressive and lethal subtype of breast cancer is triple negative breast cancer (TNBC), as evidenced with higher rates of recurrence, metastasis, and therapy resistance. However, there is lack of approved targeted therapy for the patients with TNBC. The goal of my research is to provide a novel therapeutic regimen to give benefits to the patients with TNBC. My research accomplishment during the second year (2018-2019) is continued from the first year to (1) define how BACH1 regulates mitochondrial membrane genes for metabolism of breast cancer using silencing BACH1-target genes, (2) Established whether combination treatment using hemin and metformin is effective for breast cancer treatment in xenograft models. Mitochondrial membrane genes including COX15 and UQCRC1 are direct target of BACH1 in breast cancer cells, thus silencing COX15 or UQCRC1 in BACH1-depleted cancer cells restored metformin sensitivity. Molecular mechanisms beyond is through restored NAD+ levels as well as decreased mitochondrial respiration capacity indicated as oxygen consumption rate (OCR) using Seahorse analysis. Importantly, metabolic flow of 13C-labeled glucose or glutamine was higher for glycolysis in BACH1-enriched cells relative to BACH1-depleted cells.

15. SUBJECT TERMS
BACH1 is a regulator for breast cancer metabolism. Suppression of BACH1 makes cancer cells respond well with a mitochondrial inhibitor, metformin.

16. SECURITY CLASSIFICATION OF:			17. LIMITATION OF ABSTRACT	18. NUMBER OF PAGES	19a. NAME OF RESPONSIBLE PERSON
a. REPORT	b. ABSTRACT	c. THIS PAGE			USAMRMC
U	U	U	UU	43	19b. TELEPHONE NUMBER *(include area code)*

Table of Contents

Page

1. INTRODUCTION

This research proposal is to test hypothesis that BACH1 is a metabolic regulator in breast cancer, thus targeting BACH1 rewires metabolic pathways that can be better treated with metformin. The specific aims are (1) characterize metabolic pathways regulated by BACH1 in TNBC cells; (2) define the molecular mechanisms by which BACH1 regulates mitochondrial genes; (3) analyze the efficacy of combination treatment targeting both BACH1 and mitochondrial metabolism for breast cancer. Since altered metabolic features have been a focus for cancer drug development, our finding will contribute to therapeutic development for patients with TNBC. This study propose a novel combination therapy using hemin (active ingredient of FDA-approved drug, panhematin) and metformin.

2. KEYWORDS

Triple negative breast cancer, BACH1, hemin, metformin, cancer metabolism, novel combination therapy

3. ACCOMPLISHMENTS

What were the major goals of the projects?

The major goal of this project is to develop less toxic and more specific cancer therapeutics for TNBC patients. Depletion of BACH1 either genetically or pharmaceutically drives metabolic pathways toward the mitochondrial oxidative phosphorylation that can be further a target by metformin, mitochondrial inhibitor. Using the approved metabolic drug, metformin and hemin (active ingredient of panhematin), combination of metformin and hemin will be tested using TNBC mouse models. To accomplish these goals, I propose specific aims as following;

Aim 1. Define metabolic pathways regulated by BACH1 in TNBC cells.

Aim 2. Define the molecular mechanisms by which BACH1 regulates mitochondrial genes.

Aim 3. Analyze the efficacy of treating TNBC by targeting both BACH1 and mitochondrial oxidative phosphorylation (Oxphos).

What was accomplished under these goals?

Major activities The most significant activity with research goals during this funding support was a publication of results and data that I obtained in the most prestigious peer reviewed journal, Nature. Publication entitled with "Effective breast cancer combination therapy targeting BACH1 and mitochondrial metabolism" is in **Nature, 2019, Apr;578 (7751):254-258.**

Specific objectives Specific Aim 2 was to define the molecular mechanisms by which BACH1 regulates mitochondrial metabolism in breast cancer in Year 2.

Key outcomes BACH1 in breast cancer, in particular, TNBC, is a new metabolic regulator, suppressing mitochondrial membrane gene expressions as a transcriptional repressor at their promoters, thus making cancer cells resistant to the mitochondrial inhibitor, metformin due to their metabolic pathways. Therefore, a novel combination therapy using a BACH1 inhibitor (hemin) and a mitochondrial inhibitor (metformin) effectively suppressed tumor growth in pre-clinical TNBC model. Importantly, specificity of hemin as a drug defined molecular mechanisms using hemin-resistant mutant Bach1 expressing TNBC tumors in this study, which elevated novelty.

Significant results with succinct description of the methodology according to the SOW timelines are provided as following; All the detailed information and supporting results are also provided in the journal attached in Appendix.

Specific Aim 1

Major Task 1-2- Completed in month **24.**

To determine the effect of BACH1 on central carbon metabolic flux (**Fig. 2b**), BACH1-depleted BM1 and control cells ($2x10^5$ cells/well) in 6 well plates were cultured in DMEM media containing 10 mM of uniformly labeled $^{13}C_6$ glucose (4 mM of ^{12}C glutamine), 4 mM of uniformly labeled $^{13}C_5$ glutamine (10 mM of ^{12}C glucose), or 10 mM of ^{12}C glucose/4 mM of ^{12}C glutamine for 16 hours and harvested in 80% of methanol/water in dry ice.

After a freeze/thaw cycle at -80 °C, cell supernatants were collected by centrifugation at 20,000 x *g* for 10 min and dried using a speed vac for 3 hours for the further LC/MS analysis.

A significant increase in the relative levels of TCA metabolites such as ^{13}C-labeled pyruvate and citrate/isocitrate in shBACH1 cells was observed compared to control (**Fig. 2c** and Extended data Fig. 2b. Similarly, the isotopomer distribution of [U-$^{13}C_6$]-glucose into ^{13}C-labeled citrate, alpha-ketoglutarate (αKG), fumarate, malate and other TCA intermediates was higher in shBACH1 cells (**Fig. 2d** and Extended Data Fig. 2c). These data show increased glucose flux into the TCA cycle upon BACH1 depletion.

To further study whether central carbon metabolism is affected by BACH1, tracing with [U-$^{13}C_5$]-glutamine, another carbon source for the mitochondria, was performed. As with glucose utilization, we observed a significant increase in the relative levels of citrate/isocitrate, but also saw decreased isotopomer distribution of [U-$^{13}C_5$]-glutamine into TCA intermediates in shBACH1 cells relative to control (**Fig. 2e,f** and Extended Data Fig. 2d,e). These data further indicate that BACH1 depletion reprograms the respiratory chain to be largely supported by glucose. Taken together, these results suggest that loss of BACH1 induces and promotes mitochondrial respiration and increases glucose utilization in the TCA cycle.

Fig 2b. Diagram depicting ^{13}C-metabolic flux/tracer analysis using uniformly labeled [U-$^{13}C_6$]-glucose (blue) or [U-$^{13}C_5$]-glutamine (green). The solid circle denotes ^{13}C carbon, the open circle denotes ^{12}C carbon.

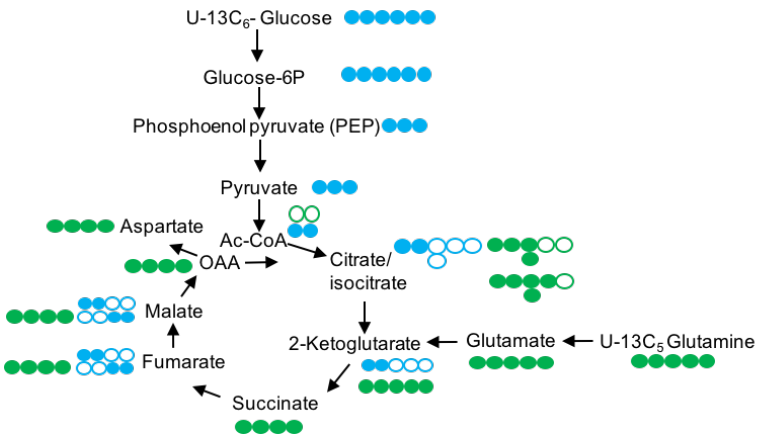

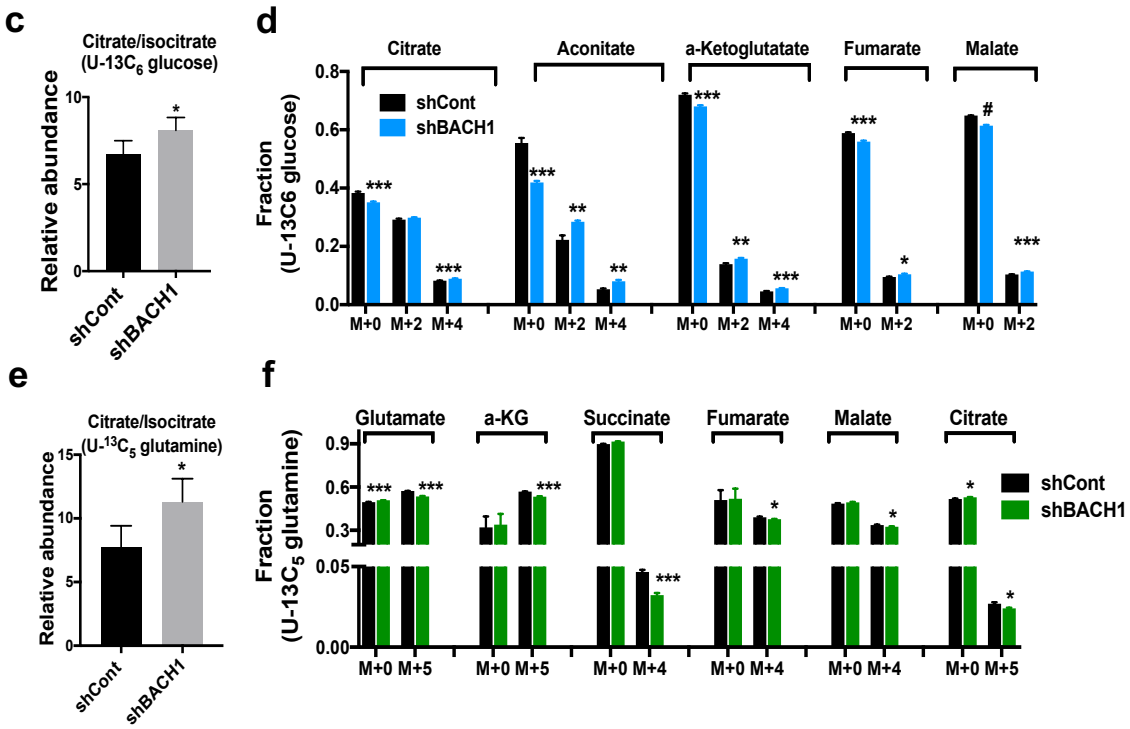

Fig. 2c-f. **Metabolic flux analyses in BACH1-depleted cancer cells. c**, **e**, Relative abundance of overall metabolite levels derived from $^{13}C_6$-glucose (**c**) or $^{13}C_5$-glutamine (**e**) in BM1-shBACH1 cells compared to control. **d**, **f**, Fractional isotopic incorporation of $^{13}C_6$-glucose (**d**) or $^{13}C_5$-glutamine (**f**) into the metabolic intermediates in glycolysis and TCA cycles is shown. M+ refers to labeled ^{13}C carbon numbers. Values are mean of 4 biological replicates ± s.e.m. with p-value (*p<0.05, **p<0.01, ***p<0.001, #p<0.0001) by two-tailed student's t-test.

Specific Aim 2

Subtask 2-Altered and Completed in month **15.**

Previous study in **Subtask 1** in Year 1 strongly indicate that BACH1 binds to promoters of target for suppress gene expression using ChIP assays. For ChIP assays, negative control using IgG as well as shBACH1 cells clearly demonstrated BACH1 specific interactions to the promoter. Also, histone modification marker for gene expression and active RNA polymerase II were incorporated for transactivation with BACH1. Since BACH1 has binding motif (ARE binding site) forming dimer with Maf proteins as Nrf proteins, BACH1 binding to the target genes are well defined. Therefore, Subtask 2 may be redundant for specificity study. Thus, I altered to mutate BACH1 molecule instead of BACH1 binding sites to study mutant BACH1 is also functional for transactivation such as transcription activation and repression in breast cancer cells.

Murine Bach1 were mutated to Alanine (A) from Cysteine (C) at Cys438, Cys464, Cys495, and Cys649 for heme binding and expressed in BM1 and MB436-shBACH1 cells. Cells expressing mut Bach1 showed stable expression of Bach1 in cells with treatment of hemin for 48 hrs (See Fig. 3d, e, f, in Attached Journal in *Appendix*). Also its transactivation was monitored using qRT-PCR, demonstrating mut Bach1 does function as wild type Bach1 for gene expression. Importantly, mut Bach1 expressing cells behave like wild type Bach1 expressing cells for their metabolism measured by OCR and ECAR using Seahorse analyzer (Extended Data **Fig 3**, See Attached Journal in Appendix).

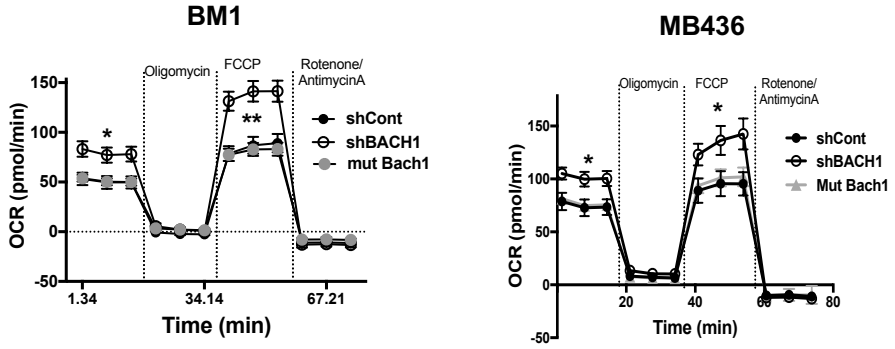

Fig. 3. Mutant Bach1 expressing cancer cells

MB436 cells transiently transfected with Mut-Bach1 (100 ng) in MB436-shBACH1 or BM1-shBACH1 cells were used for measurement of OCR along with BACH1 depleted cells or BACH1 intact cells as control. Data are mean ± s.e.m. (n=6) with p-value (*p<0.05, N.S: not significant) by two-tailed student's t-test.

Subtask 3-Completed in month **18.**

Since BACH1 loss increases utilization of the mitochondria as a source of energy and biosynthetic precursors, these cells might exhibit increased NAD^+/NADH ratios, consistent with changes in mitochondrial function. We also added pyruvate (2.5 mM) to BACH1-depleted cells and found that pyruvate further increased NAD^+/NADH ratios and prevented metformin from inhibiting cell growth in BACH1-depleted cells, consistent with the role of BACH1 in altering mitochondrial metabolism (Extended Data **Fig. 4a**).

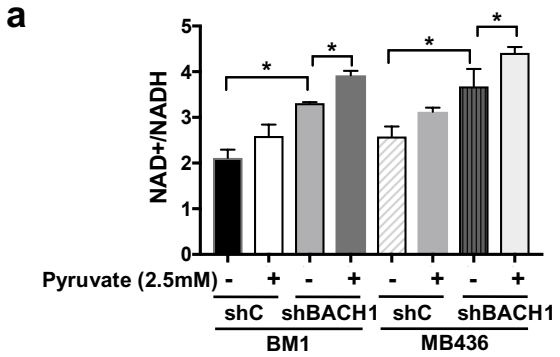

Fig. 4a. Relative NAD^+/NADH ratios in BM1 or MB436 cells expressing control or shBACH1. Values are mean ± s.e.m of 3 biological replicates with p-values (*p<0.05) by two-tailed student's t-test. NAD(H) was measured using the NAD+/NADH-Glo Assay kit (Promega, G9071) in accordance with the manufacturer's protocol.

Rewired metabolic pathways by BACH1 depletion that I revealed showed increased glucose utilization for mitochondrial metabolism rather than glycolysis. Therefore, I focused on the entry point of carbon substrate into TCA cycle by analyzing pyruvate dehydrogenase (PDH) that converts pyruvate to acetyl CoA and pyruvate kinase (PDK) which inhibits PDH by phosphorylating ser293 of PDH. **(Addition to Subtask 3.)** BACH1 knockdown reduces both PDK and pSer293-PDH but not overall PDH levels, thereby up-regulating PDH activity (**Fig. 2g,h** and Extended Data Fig. 2h). ChIP assays showed that BACH1 binds to the promoters of *PDK* genes in BM1 and MB436 but not BACH1-deficient MB468 cells (**Fig. 2i** and Extended Data Fig. 2i). These results indicate that BACH1 regulates PDK transcription and PDH phosphorylation, key steps controlling glycolysis and mitochondrial metabolism.

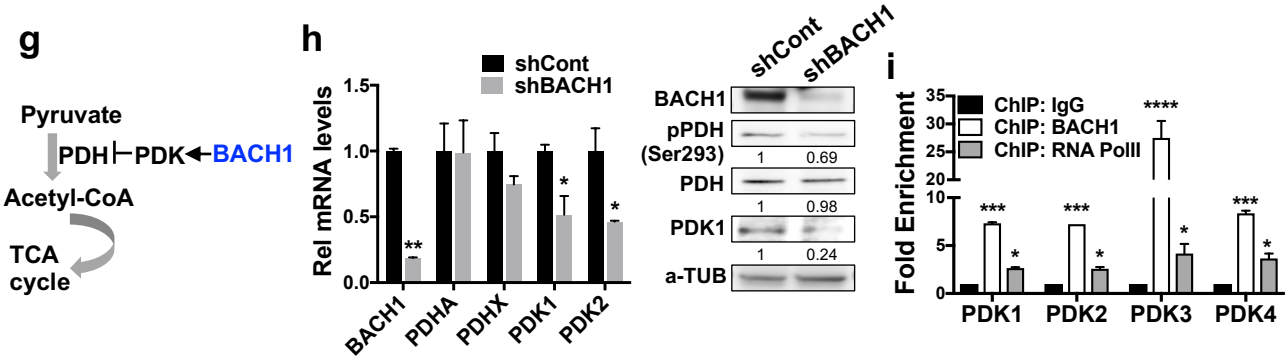

Fig. 2g-i. Pyruvate dehydrogenase (PDH) is regulated by BACH1 for metabolic pathways.
g, Diagram showing BACH1 regulation of PDK and PDH. **h**, Relative mRNA of PDK and PDH genes and western blots of protein levels of PDK, PDH, and phosphorylated PDH (Ser293) in BM1-shBACH1 (#1) and its control cells. Western blots are representative images of more than three independent assays. Band density generated using a Licor Odyssey Fc is shown below the blots. **i**, Relative BACH1 and RNA Polymerase II enrichment in the promoter regions of PDK genes compared to IgG binding using BM1 cells. Values are mean ± s.e.m of at least three independent assays with p-values (*p<0.05, ***p<0.001, ****p<0.0001) determined by two-tailed student's t-test.

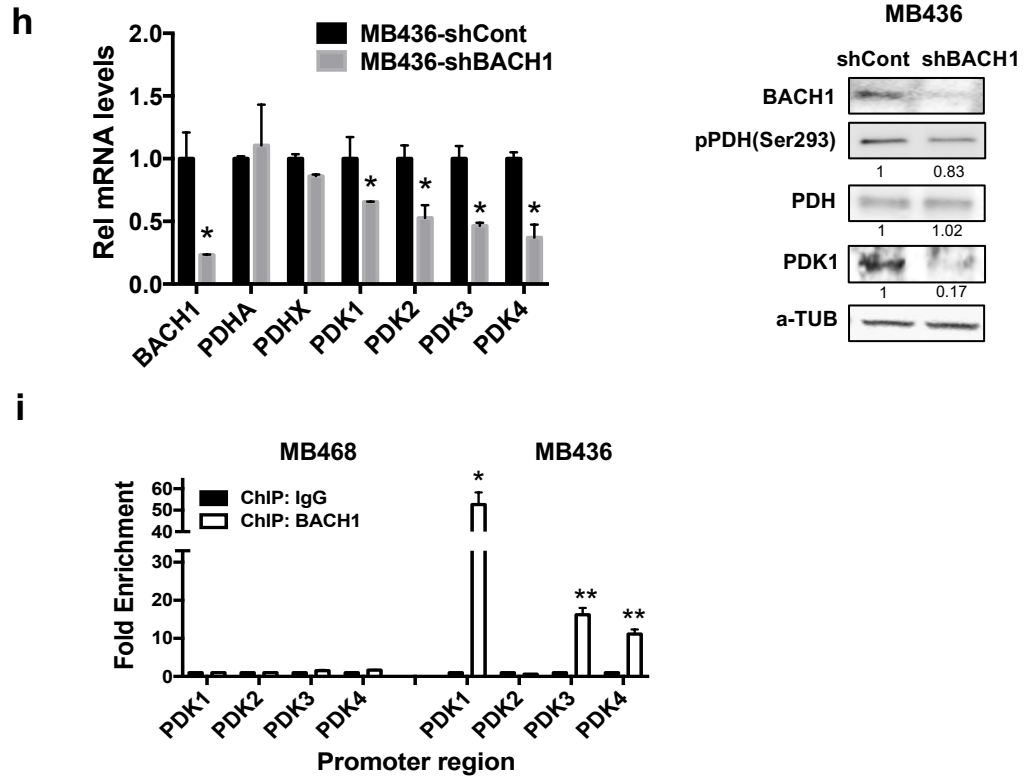

Fig. 2h-i. Expression of PDK levels and p-PDH in shBACH1 cells.
h, Relative mRNA and protein levels of PDH and PDK genes in MB436-shBACH1 cells compared to wild type control. qRT-PCR values represent mean of three biological replicates ± s.e.m with p-value (*p<0.05) determined by two-tailed student's t-test. Representative images of westeern blots probed with antibodies to proteins as indicated are shown. Band density generated using a Licor Odyssey Fc is shown below the blots. **i**, ChIP assays showing fold enrichment of BACH1 recruitment to PDK genes using MB436 and MB468 cells. Values represent mean of three independent assays ± s.e.m; *p<0.05, **p<0.01 determined by two-tailed student's t-test.

Specific Aim 2

Subtask 4- Completed in month **21**.

The mitochondrial ETC genes (*COX15* and *UQCRC1*) induced in BACH1 depleted cells and also required for metformin sensitivity were determined to see effect on metformin sensitivity. Detailed methods are as following: siRNAs for UQCRC1 (Human UQCRC1 Flexi tube siRNA, SI00051275, Qiagen), COX15 (Human COX15 6flexi Tube siRNA, SI014180911, Qiagen), or siRNA control (Universal Scrambled negative control siRNA, SR30004, Origene) were transfected into breast cancer cells with Lipofectamine 3000 (Invitrogen) in OPTI-MEM overnight for *in vitro* assays. For in vitro growth assays, breast cancer cells (5-8×10^3 cells/well) were plated on 96-well plates to observe growth of cells every 4 hours by phase contrast imaging and shown as % confluence of area covered by cells using an IncuCyte Zoom Live Cell Analysis system (Essen Bioscience). After 24 hours of plating, inhibitors were added and monitored until control cells reached 100 % confluence. 100% confluence refers to complete coverage of the plates by cells. To determine cell viability, cells were seeded in black walled 96-well plates overnight and treated with inhibitors. After 48 hours, cells were treated with Calcein AM (R&D system) in PBS for 1 hour at 37 °C to measure absorbance with excitation at 420 nm and emission at 520 nm using a Victor3 plate reader (PerkinElmer). The absorbance was used to reflect live cell numbers and was normalized to those in control or with vehicles and shown as relative viability (%).

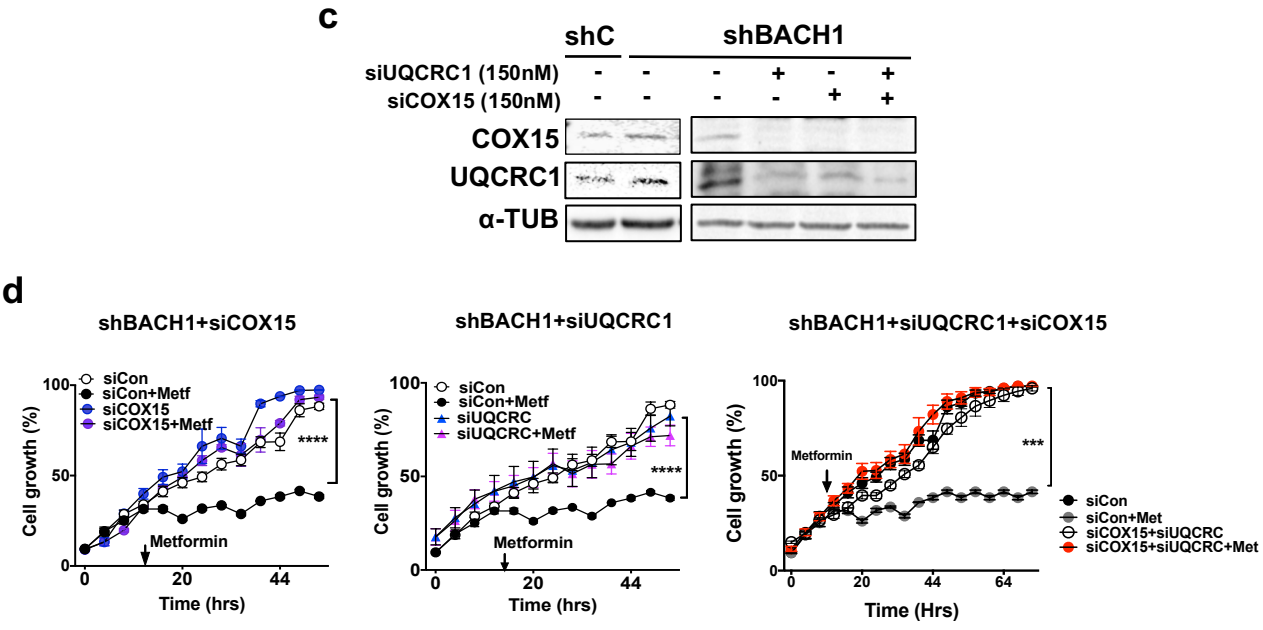

Fig. 4c-d. Effect of mitochondrial genes (COX15 and UQCRC1) on metformin sensitivity. c, Western blots of COX15, UQCRC1 and a-TUBULIN using lysates from BM1-shBACH1 cells transfected with siCOX15 and siUQCRC1 using lipofectamin2000. **d**, Cellular growth (%) of BM1-shBACH1 cells transfected with siRNA for *COX15* and/or *UQCRC1* and treated with metformin (10 mM) using IncuCyte Zoom (Essen Biosciences).

As evidenced in Fig 4c and d, The mitochondrial ETC genes induced in BACH1-depleted cells were responsible for metformin sensitivity. Silencing of *COX15* or *UQCRC1* in BACH1-depleted cells completely restored metformin resistance and rescued cell growth (Extended Data **Fig. 4c, d**). Notably, neither expression of the metformin transporter (OCT1)[31] nor mitochondrial biogenesis genes such as peroxisome proliferator-activated receptor gamma (PPARγ) or peroxisome proliferator-activated receptor gamma coactivator1-alpha (PGC1α) were altered by BACH1 depletion (Extended Data Fig. 4e in *Appendix*). Together, these results demonstrate that increased mitochondrial ETC gene expression enhances sensitivity to ETC inhibitor treatment.

Specific Aim 3.
Major Task 3-2.
Subtask 1- completed in month **16**.
One of the TNBC Genetically engineered mouse (GEM) model, C3(1)/Tag that I proposed to use for my study. TNBC mouse model, C3(1)/Tag were bred in house to obtain ample number of mice for analyses. Initially, tumor development was observed at age of 12-14 weeks (n=18 total) with ductal carcinoma in situ (DCIS). Later, tumors developed and grew to a palpable size with caliper measurement at age 16-18 weeks. When tumors reach maximum growth size (1 g), tumors about age 22-24 weeks, tumors were isolated from mice for further analyses.

Surprisingly, tumors isolated from C3(1)/Tag mice do not express sufficient BACH1 levels compared to other TNBC models when I analyzed BACH1 expression (**Fig. 5**). Therefore, C3(1)/Tag mouse model will not be adequate for my future study.

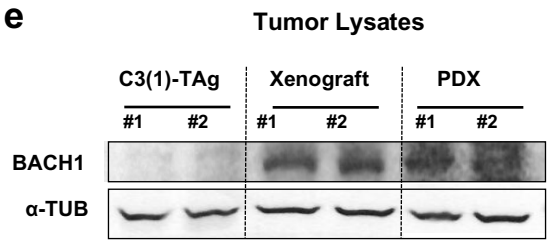

Fig 5. BACH1 expression across tumor type such as C3(1)/Tag, BM1 xenograft, and PDX tumors.
Tumor lysates isolated from individual mouse (#1 and #2) in each models were used for western blots against BACH1 and alpha-Tubulin using LyCor Odyssey image.

Similarly, breast cancer cells isolated from the C3(1)/Tag mice are M6C cell lines, which shows low levels of BACH1, thus making cells highly sensitive to single metformin treatment (*See Annual Summary 2018*).

Major Task 3-2.
Subtask 2- altered and completed in month **20**.

Since both C3(1)/Tag mouse model and M6C cell lines are not efficient to dedicate efficacy of combination therapy since BACH1 is already low. Therefore, I altered Subtask 1 to investigate specificity of BACH1-inhibitor, Panhematin, by creating heme-resistance mutant Bach1 using two human TNBC cells lines that express BACH1 (MDA-MB-436 and BM1). Because drug specificity is essential for translational investigation, and the future goal of this study is for patient care. Heme-resistant murine Bach1 (mut-Bach1) expressing breast tumors are intensively useful to validate any off-target effects by Panhematin. Notably, Panhematin is a FDA-approved drug for the porphyria to fix heme homeostasis.

Mut-Bach1 has cysteine to alanine point mutations in 4 C-terminal heme binding sites that are implicated in heme binding and release of BACH1 from DNA for nuclear export and subsequent degradation (Fig. 3d, e in *Appendix*). Heme binding dipeptide motifs (CP) of Bach1 were mutated to Alanine (A) from Cysteine (C) at Cys438, Cys464, Cys495, and Cys649 (Thermo Fisher) and cloned into pCDNA3.1 and sequenced for mammalian cell transduction using Lipofectamine 3000 (Invitrogen). For expression of mut-Bach1 or wt-Bach1 in stable cell lines, mut-Bach1 and wt-Bach1 sequences were cloned into pCDH for lentiviral transfection.

Interestingly, mut-Bach1 expressed in shBACH1 TNBC cells rescues the effect of BACH1 depletion on ETC gene transcription, OCR, ECAR and metformin inhibition of cell growth and viability (Fig. 3f, g and Extended Data 6a, b: *See attached journal in Appendix*). However, in contrast to control or shBACH1 cells transfected with wt-Bach1, mut-BACH1-expressing cells were resistant to hemin treatment with respect to metabolic properties and metformin sensitivity (**Fig. 6** and Extended Data Fig. 6c-e, *See attached journal in Appendix*). These data suggest that hemin acts through specific degradation of BACH1.

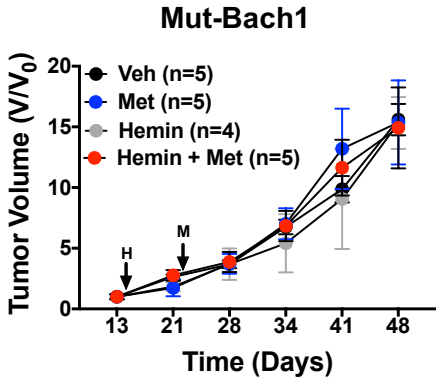

Fig. 6. Plot of relative tumor volume of mice (n=4-5/group) xenografted with mut-Bach1 expressing cells and treated with hemin and metformin (300 mg/kg/day). For all xenograft tumors, 2 x 10^6 of TNBC cells were injected into a fat pad per mouse to form tumors. When palpable size of tumors (30-50 mm^3) was detected, hemin (50 mg/kg/day) was administered daily by intraperitoneal injection (H:hemin) and metformin (200 mg/kg/day) in drinking water (M:metformin) was provided *ad libitum* until the end of experiments. Tumors are measured weekly by caliper and shown as mean ± s.e.m.

What opportunities for training and professional development has the project provided?

1. **American Association for Cancer Research (AACR) Tumor Immunology and Immunotherapy** at Miami Beach, FL (Nov. 27-30, 2018). I, PI, attended scientific conference held by AACR for tumor immunology and immunotherapy to gain insights into tumor immunology for future research.

How were the results disseminated to communities of interest?

1 News for communities in public issued on March 6, 2019. (See; https://www.uchicagomedicine.org/forefront/cancer-articles/2019/march/old-drugs-bring-new-hope-to-a-cancer-that-lacks-precision-therapy) , and https://news.uchicago.edu/story/repurposing-older-drugs-could-raise-new-hope-breast-cancer-treatment.

2. MedicalXpress (Mar. 6. 2019), See https://medicalxpress.com/news/2019-03-drugs-cancer-lacks-precision-therapy.html

3. EureKAlert by AAAS (Mar. 6. 2019), https://www.eurekalert.org/pub_releases/2019-03/uocm-odb030119.php,

4. Newswise (Mar. 6. 2019), https://www.newswise.com/articles/old-drugs-bring-new-hope-to-a-cancer-that-lacks-precision-therapy,

5. ecancer, with title "Old drugs bring new hope to a cancer that lacks precision therapy" (Mar. 6. 2019) see; https://ecancer.org/news/15570-old-drugs-bring-new-hope-to-a-cancer-that-lacks-precision-therapy.php,

6. SpecialtyPharmacyTimes.com (March. 21. 2019) released news on our publication with title "Novel, Repurposed Drug Combo Shows Potential in Triple-Negative Breast Cancer" see; https://www.specialtypharmacytimes.com/news/novel-repurposed-drug-combo-shows-potential-in-triple-negative-breast-cancer

7. NatureAsia.com. (Apr. 11. 2019) see http://www.natureasia.com/ko-kr/nature/highlights/98317

What do you plan to do during the next reporting period to accomplish the goals?

- As I proposed in original SOW, I will follow the work flow with time lines. Major task 3 to test efficacy of combinational treatment of hemin and metformin on human patient tumor-derived xenograft (PDX) tumors. A few of PDX lines were tested in Year 2, but will be intensively examined for further analyses using the RNA-sequencing data sets from patients and the biochemical assays to screen BACH1 expression levels. Established PDX tumor models are very useful tools for translational research including a novel combination therapy of hemin and metformin to validate our findings and to further utilize our findings for the new therapeutics of breast cancer patients.

4. IMPACT

What was the impact on the development of the principal discipline(s) of the project?

This proposal has impact on development of novel combination therapy to enhance efficacy of metformin, a drug, that is most prescribed for diabetic patients to treat at high-risk breast cancer patients. Research data that I obtained present that targeting BACH1 generates a synthetic lethality for cancers that are not responsive to metformin treatment. Molecular mechanism beyond is through changes of metabolism of cancer cells by BACH1 reduction, which results in the state of cancer cells responding well to the drug, metformin.

Accomplishment in **Year 2** defined that BACH1 rewires metabolic pathways of glucose in cancer cells. Upon depletion of BACH1 in breast cancer cells, flux tracing analyses using labeled-glucose (^{13}C-glucose) revealed reduced glycolysis concomitant increased mitochondrial oxidative phosphorylation, which is consistent with biochemical metabolic assays using Seahorse XF analyzer. Accordingly, ATP production and lactate production was reduced upon BACH1 depletion, while NAD+/NADH levels were increased due to compensatory enhanced mitochondrial metabolism. Molecular mechanisms by which BACH1 regulates cancer metabolism are through directly suppressing mitochondrial membrane genes by BACH1 as a transcriptional suppressor in cancer cells. Silencing of mitochondrial membrane genes including COX15 and UQCRC1 which are BACH1 targets recovered metformin resistance, indicating direct acts of BACH1 on mitochondrial metabolism. In addition, the key enzyme connecting glycolysis to the TCA cycle, pyruvate dehydrogenase (PDH) that converts pyruvate to acetyl CoA and pyruvate kinase (PDK) which inhibits PDH by phosphorylating ser293 of PDH, were directly regulated by BACH1.

Importantly, BACH1 depletion achieved by active ingredient of a FDA-approved drug, hemin, in TNBC mouse tumors was effective to render drug sensitivity to metformin showing significantly reduced tumor growth in the *in vivo* mouse model study. Analyses for efficacy of combinational treatment targeting both BACH1 and mitochondrial oxidative phosphorylation using xenograft mouse models had been validated in Year 1. Furthermore, specificity of the hemin in cancer cells were validated showing that hemin acts through specific degradation of BACH1 in biochemical assays using mutant Bach1 and in vivo tumor model expressing mut-Bach1 in Year 2. Accomplishment in Year 2 supports our finding in Year 1 as well as enhanced novelty of our study.

What was the impact on other disciplines?

"Nothing to Report."

What was the impact on technology transfer?

This novel combination therapy has immediate commercial technology or public uses to treat breast cancer patients that are useful to initiate a start-up company or clinical trials. Also our finding has potential to be applied to other types of cancers expressing high BACH1 such as ovary, liver, prostate, and pancreas based on the patient data.

What was the impact on society beyond science and technology?

"Nothing to Report."

5. CHANGES/PROBLEMS

Changes in approach and reasons for change

Specific Aim 2, subtask 2 and 3 were changed to mutate Bach1 instead its binding site to understand the molecular mechanism how the drug, hemin, works on Bach1 in cancer cells. Because the molecular mechanisms by which BACH1 regulates target genes were clearly well defined using number of assays including quantitative PCR, western blotting as well as chromatin immunoprecipitation (ChIP) assays in Year 1. For all those molecular biology analyses, BACH1-depleted cells as well as IgG were used as a negative control, showing direct regulation by BACH1 at the promoter regions for gene expression regulation. Importantly, histone modification marker (H3K27me3) and active RNA polymerase II were adapted for ChIP assays for indication of gene activation by BACH1 recruitment. Thus, subtask 2 was altered to study mutant Bach1 instead of mutated Bach1 binding sites.

Also there was technical issues in Subtask 3. Silencing COX15 and/or UQCRC1 using siRNA is too transient (up to 72 – 84 hours) to be further analyzed in timely manner. Silencing COX15 or UQCRC1 using siRNA for overnight (24 hours) and transplanted into 96 well plate for overnight (24 hours), and transferred to Seahorse analyzer overnight for stabilization (24 hours) took already 72 hours before analysis with inhibitors. All cells lost siRNA expression at the end of analysis. Subtask 3 is to determine whether these targets are essential to generate metabolic phenotypic changes in breast cancer, so viability assays using cells that are silenced with COX15 and/or UQCRC1 are valid in subtask 4. Instead, I examined whether hemin effect is directly on BACH1 in tumors. First, cysteine residues at Cys438, Cys464, Cys495, and Cys649 in the hemin-binding motifs at the C-terminus were mutated to Alanine in murine Bach1. This mutant Bach1 (Mut-bach1) was stably expressed in human TNBC cells, constitutively expressing mut-Bach1 even with long term hemin treatment. Biochemical assays using this mut-Bach1 expressing TNBC cells were tested for metabolic functions using Seahorse XF analyzer to show whether they rescue mitochondrial respiration showing reduced oxygen consumption rate (OCR), and ECAR compared to wild type control cells. Also, mut-Bach1 cells were used for in vitro viability and growth assays using CaAM staining and IncuCyte Zoom, respectively, to clarify these cells are resistant to Metformin treatment with respect to hemin treatment.

Specific Aim 3, Subtask 2 was changed because C(3)-Tag mouse model and its derivative cell lines (M6C cells) were inadequate for this research. Both C(3)-Tag mouse and M6C cells express too low Bach1 to test the combination therapy targeting Bach1. Since the impact and significance of this research proposal is on novel, less toxic cancer therapeutics to benefit patients with TNBC using two FDA-approved drugs, I alternatively used drug-resistant mouse models (xenograft tumor model expressing heme-resistant mutant Bach1 in MDA-MB-436 and BM1) for Subtask 2. Since drug specificity is essential for translational research, changed subtask 2 in Specific Aim 3 strengthened molecular mechanisms of Bach1 as a novel therapeutics. Heme-resistant murine Bach1 (mut-Bach1) expressing breast tumors are intensively useful to validate any off-target effects by Panhematin. Notably, Panhematin is a FDA-approved drug for the porphyria to fix heme deficiency. Taken together, I obtained very useful data suggesting that hemin acts through specific degradation of BACH1 in breast tumor.

Actual or anticipated problems or delays and actions or plans to resolve them
There was no problems or delays of plans since I had completed changed subtasks.

Changes that had a significant impact on expenditures
I substituted cell lines from transiently silenced siCOX and/or siUQCRC1 shBACH1 cells to mut-Bach1 cells instead, in order to test metabolic functions, thus there was no impact on expenditures.

Significant changes in use or care of human subjects
"Nothing to Report."

Significant changes in use or care of vertebrate animals
I substituted only mouse models from GEM models to xenografted tumor models expressing mut-Bach1 for a combination therapy using hemin and metformin, thus there was no impact on total expenditure. All the methods including number of mouse per treatment group and consistent treatment conditions such as drug dosages and duration of treatment for Subtask 1 were consistent as planned, thus resulted in no impact on expenditure.

Significant changes in use or care of biohazards, and/or select agents
"Nothing to Report."

6. PRODUCTS

- **Journal Publications**

1. Jiyoung Lee, Yesilkanal AE, Wynne JP, Frankenberger C, Liu J, Yan J, Elbaz M, Rabe DC, Rustandy FD, Tiwari P, Grossman EA, Hart PC, Kang C, Sanderson SM, Andrade J, Nomura DK, Bonini MG, Locasale JW, Rosner MR. ; Effective breast cancer combination therapy targeting BACH1 and mitochondrial metabolism; Nature; 568 (7751); 2019; 254-258; Published; Acknowledgement of federal support (Yes).

- **Presentations**

1. Keystone Cancer Metastasis international meeting: The role of metabolism, Immunity and the microenvironment Metabolism Meeting
   Florence, Italy (Mar. 15-19, 2019)
   Title: Effective combination therapy for breast cancer targeting BACH1 and mitochondrial metabolism.

2. American Association for Cancer Research (AACR) Annual Meeting
   Atlanta, GA (Mar. 29-Apr.03, 2019)
   Title: Effective combination therapy for breast cancer targeting BACH1 and mitochondrial metabolism.

- Website(s) or other Internet site(s)
  "Nothing to Report."
- Technologies or techniques
  "Nothing to Report."
- Inventions, patent applications, and/or licenses
  "Nothing to Report."
- Other products
  "Nothing to Report."

7. PARTICIPANTS & OTHER COLLABORATING ORGANIZATIONS

What individuals have worked on the project?

Name:	Jiyoung Lee
Project Role:	"no change"
Research Identifier	"no change"
Nearest person month worked:	"no change"
Contribution to project	"no change"
Funding Support:	"no change"

Has there been a change in the active other support of the PI(s) or senior/key personnel since the last reporting period?
"Nothing to Report."

What other organizations were involved as partners?
"Nothing to Report."

8. SPECIAL REPORTING REQUIREMENTS
"Nothing to Report" during this reporting period.

9. APPENDICES
A journal published as a major accomplishment in 2019 is attached (See page 17-42).

LETTER

https://doi.org/10.1038/s41586-019-1005-x

Effective breast cancer combination therapy targeting BACH1 and mitochondrial metabolism

Jiyoung Lee[1], Ali E. Yesilkanal[1], Joseph P. Wynne[1], Casey Frankenberger[1], Juan Liu[2], Jielin Yan[1], Mohamad Elbaz[1], Daniel C. Rabe[1], Felicia D. Rustandy[1], Payal Tiwari[1], Elizabeth A. Grossman[3,4,5], Peter C. Hart[6], Christie Kang[6], Sydney M. Sanderson[2], Jorge Andrade[7], Daniel K. Nomura[3,4,5], Marcelo G. Bonini[6,8], Jason W. Locasale[2] & Marsha Rich Rosner[1]*

Mitochondrial metabolism is an attractive target for cancer therapy[1,2]. Reprogramming metabolic pathways could improve the ability of metabolic inhibitors to suppress cancers with limited treatment options, such as triple-negative breast cancer (TNBC)[1,3]. Here we show that BTB and CNC homology1 (BACH1)[4], a haem-binding transcription factor that is increased in expression in tumours from patients with TNBC, targets mitochondrial metabolism. BACH1 decreases glucose utilization in the tricarboxylic acid cycle and negatively regulates transcription of electron transport chain (ETC) genes. BACH1 depletion by shRNA or degradation by hemin sensitizes cells to ETC inhibitors such as metformin[5,6], suppressing growth of both cell line and patient-derived tumour xenografts. Expression of a haem-resistant BACH1 mutant in cells that express a short hairpin RNA for *BACH1* rescues the BACH1 phenotype and restores metformin resistance in hemin-treated cells and tumours[7]. Finally, *BACH1* gene expression inversely correlates with ETC gene expression in tumours from patients with breast cancer and in other tumour types, which highlights the clinical relevance of our findings. This study demonstrates that mitochondrial metabolism can be exploited by targeting BACH1 to sensitize breast cancer and potentially other tumour tissues to mitochondrial inhibitors.

The lack of approved targeted therapies and effective chemotherapy with low toxicity for TNBC remains a major hindrance for treatment and prompted us to identify novel targets[8]. Using a bioinformatics approach based on patient-derived data, we showed that the transcription factor BACH1 is required for metastasis of aggressive TNBCs, and its gene signature is associated with poor outcomes[9–12]. Of note, *Bach1*-null mice are viable and develop normally[13], which suggests that BACH1 may be a good target for cancer therapy because it controls cellular stress responses but is not essential—and therefore may be inhibited with few side effects. Analyses of *BACH1* transcript and gene copy number in primary tumour datasets (The Cancer Genome Atlas (TCGA)[14], Molecular Taxonomy of Breast Cancer International Consortium (METABRIC)[15], GSE2034[16] and GSE11101[17]) showed a significant gain in triple-negative and basal-like breast cancer relative

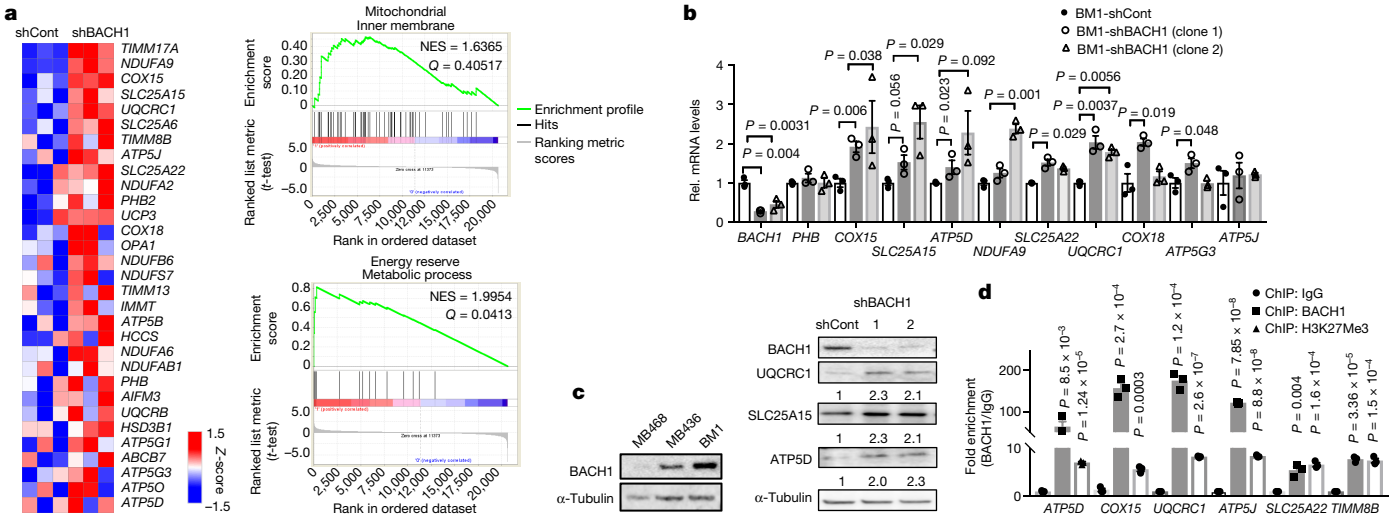

Fig. 1 | BACH1 inhibits mitochondrial genes in TNBC. a, Gene set enrichment analysis of BACH1-regulated genes with normalized enrichment score (NES) and false-discovery rate (FDR) *Q* value; heat map depicts changes in gene expression levels involved in 'mitochondrial inner membrane', based on microarray data from BM1-shBACH1 and control cells ($n = 3$ biological replicates per cell line). Synonyms shown for: *ATP5F1B* (*ATP5B*), *ATP5MC1* (*ATP5G1*), *ATP5MC3* (*ATP5G3*), *ATP5PO* (*ATP5O*) and *ATP5F1D* (*ATP5D*). **b**, Left, relative mRNA levels of mitochondrial inner membrane genes in BM1-shBACH1 cells (two shBACH1 vectors) compared to the wild-type control (BM1-shCont) measured by qRT–PCR. Mean ± s.e.m., $n = 3$ biological independent replicates, two-tailed *t*-test. Right, protein blots of BACH1 and ETC genes in BM1-shBACH1 and control cell lysates. Relative band density shown below the blots. **c**, Representative BACH1 western blots using lysates of MB468, MB436 or BM1 cells. Each experiment repeated independently more than three times with similar results. **d**, Recruitment of BACH1 and H3K27Me3 to promoter regions of mitochondrial genes in BM1 cells. Relative fold enrichment compared to IgG binding shown as mean ± s.e.m., $n = 3$ biologically independent replicates, two-tailed *t*-test.

[1]Ben May Department for Cancer Research, University of Chicago, Chicago, IL, USA. [2]Department of Pharmacology and Cancer Biology, Duke University, Durham, NC, USA. [3]Department of Chemistry, Molecular and Cell Biology, and Nutritional Sciences and Toxicology, University of California at Berkeley, Berkeley, CA, USA. [4]Department of Molecular and Cell Biology, University of California at Berkeley, Berkeley, CA, USA. [5]Department of Nutritional Sciences and Toxicology, University of California at Berkeley, Berkeley, CA, USA. [6]Department of Medicine, University of Illinois at Chicago, Chicago, IL, USA. [7]Center for Research Informatics, University of Chicago, Chicago, IL, USA. [8]Present address: Department of Medicine, Medical College of Wisconsin, Milwaukee, WI, USA. *e-mail: m-rosner@uchicago.edu

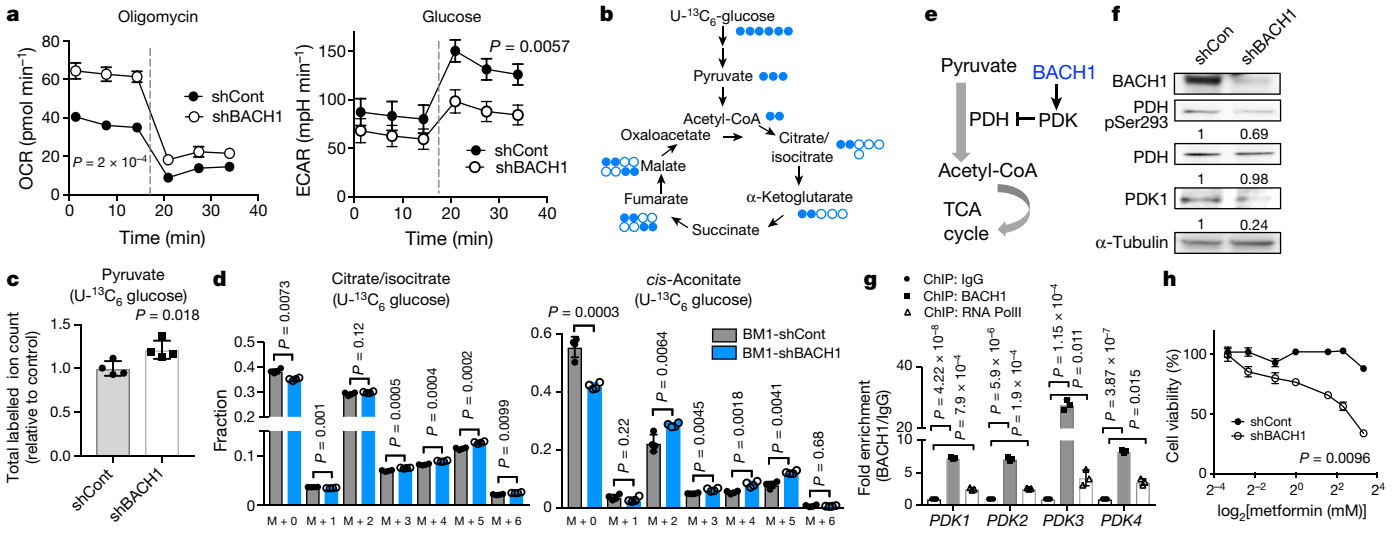

Fig. 2 | BACH1 regulates mitochondrial metabolism. a, Measurement of OCR (left) and ECAR (right) in control and BM1-shBACH1 cells. Mean ± s.e.m., $n = 6$ biologically independent samples, two-tailed t-test. **b**, Schematic of simplified ^{13}C-metabolic-tracer analysis using uniformly labelled [U-$^{13}C_6$]-glucose. Solid circle, ^{13}C; open circle, ^{12}C. **c**, Relative total labelled ion counts derived from $^{13}C_6$-glucose in BM1-shBACH1 cells compared to control. **d**, Fractional isotopic incorporation of $^{13}C_6$-glucose into representative intermediates in TCA cycles as shown. M, number of labelled carbons. In **c**, **d**, mean ± s.e.m., $n = 4$ biologically independent samples, two-tailed t-test. **e**, Schematic showing BACH1 regulation of PDK and PDH. **f**, Relative expression of PDK and PDH in BM1-shBACH1 (clone 1) and control cells. Western blots shown are representative images of more than three independent assays. Relative band density shown below the blots. **g**, Relative BACH1 and RNA polymerase II (Pol II) enrichment in promoter regions of PDK genes compared to IgG binding, in BM1 cells. Mean ± s.e.m., $n = 3$ biologically independent samples, two-tailed t-test. Three independent experiments repeated with similar results. **h**, Cell viability of BM1-shBACH1 or BM1 control cells treated with or without metformin for 48 h. Mean ± s.e.m., $n = 6$ biologically independent samples, two-tailed t-test.

to other subtypes such as luminal A, luminal B, HER2-enriched and normal-like breast cancer (Extended Data Fig. 1a, b).

To examine other potential functions of BACH1 in TNBC, we evaluated microarrays of metastatic MDA-MB-231-derived cells (BM1; also termed 1833 (ref. [18])) expressing short hairpin RNA (shRNA) for *BACH1* (BM1-shBACH1) or control vector (BM1-shCont)[10]. Gene enrichment analysis identified a significant increase in metabolic pathways including energy metabolism and mitochondrial inner membrane genes upon BACH1 depletion (Fig. 1a and Extended Data Fig. 1c). We validated shBACH1 induction of mitochondrial inner membrane genes largely involved in the ETC by quantitative reverse transcription with PCR (qRT–PCR) and immunoblotting using two human TNBC cell lines that express BACH1: BM1 and MDA-MB-436 (MB436) (Fig. 1b and Extended Data Fig. 1d).

To determine whether mitochondrial genes are direct BACH1 targets, we analysed potential BACH1 recruitment sites (MAF recognition elements) within the promoter regions of these genes[19]. Having identified potential BACH1-binding sites in six mitochondrial genes, *ATP5D* (also known as *ATP5F1D*), *COX15*, *UQCRC1*, *ATP5J* (also known as *ATP5PF*), *SLC25A22* and *TIMM8B* (Extended Data Fig. 1e), we performed chromatin immunoprecipitation (ChIP) assays with BACH1 antibody[20]. Haem oxygenase 1 (*HMOX1*), which is transcriptionally repressed by BACH1[13], or BACH1-low cells (shBACH1 or MB468) served as positive or negative controls for BACH1-binding specificity (Fig. 1c and Extended Data Fig. 1f). We observed a marked enrichment of BACH1 binding to the promoter regions of ETC genes and binding of the repressive histone marker H3K27Me3[21] (Fig. 1c, d and Extended Data Fig. 1g, h). These results suggest that BACH1 is a direct suppressor of mitochondrial ETC gene transcription.

Further bioinformatics analyses using data from patients with breast cancer supported these findings. Kyoto Encyclopedia of Genes and Genomes (KEGG) analysis of genes that negatively correlate with BACH1 expression in multiple breast cancer datasets showed a marked enrichment in oxidative phosphorylation gene expression as well as genes associated with other diseases (Extended Data Fig. 1i, j). Furthermore, expression of ETC genes in TNBC-specific TCGA datasets was inversely correlated with BACH1 expression (Extended Data Fig. 1k and Supplementary Table 1).

We then determined whether the BACH1-induced changes in ETC genes affect metabolic phenotypes in breast cancer cells by measuring both oxygen consumption rate (OCR), an indication of aerobic respiration, and extracellular acidification rate (ECAR), a readout of lactic acid produced from aerobic glycolysis. TNBC cells depleted of BACH1 displayed increased basal as well as maximum OCR but decreased ECAR relative to the control (Fig. 2a and Extended Data Fig. 2a). These data suggest that loss of BACH1 promotes mitochondrial respiration.

Consistent with these results, mass-spectrometry analysis of metabolites identified increased levels of TCA cycle intermediates and ATP levels upon BACH1 knockdown (Extended Data Fig. 2b). We also observed a decrease in the steady-state levels of multiple intermediates in the glycolysis pathway, including glucose-6-phosphate (G6P), fructose-6-phosphate (F6P), fructose-1,6-bisphosphate (F16BP), dihydroxyacetone phosphate/glyceraldehyde 3-phosphate (DG3P) and lactate in shBACH1 cells.

To determine the effect of BACH1 on glucose utilization, we first treated shBACH1 cells with uniformly labelled [U-$^{13}C_6$]-glucose[22] (Fig. 2b). We observed a significant increase in the levels of ^{13}C-labelled pyruvate in shBACH1 cells compared to control (Fig. 2c). Similarly, the isotopomer distribution of [U-$^{13}C_6$]-glucose into ^{13}C-labelled citrate, aconitate, α-ketoglutarate, fumarate and malate generally displayed a small but significant increase in shBACH1 cells relative to control cells (Fig. 2d and Extended Data Fig. 2c). A decrease in the labelling of the glycolytic intermediates ^{13}C-G6P and ^{13}C-glycerol-3-phosphate was also observed in shBACH1 cells relative to controls. We performed additional tracing with [U-$^{13}C_5$]-glutamine, an alternative carbon source for mitochondria. In contrast to glucose utilization, we observed a small but significant decrease in isotopomer labelling of [U-$^{13}C_5$]-glutamine in TCA intermediates upon BACH1 depletion (Extended Data Fig. 2d). Collectively, these results suggest that loss of BACH1 induces ETC gene expression, promotes mitochondrial respiration and increases glucose utilization in the TCA cycle.

To better understand the changes in mitochondrial metabolism upon BACH1 depletion, we analysed an entry point into the TCA cycle,

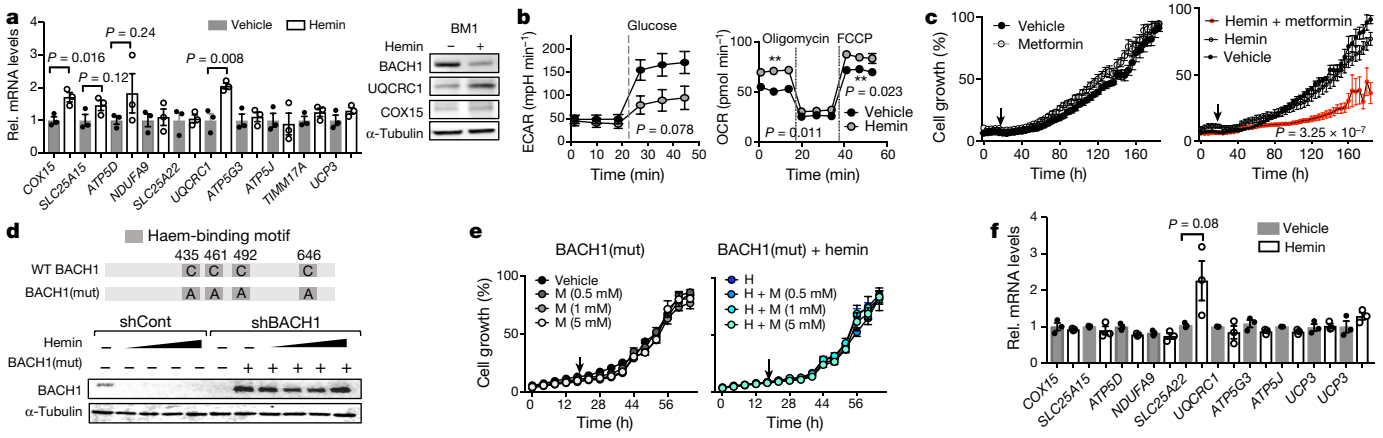

Fig. 3 | Hemin mimics shBACH1 through BACH1 degradation in TNBC. a, Relative mRNA levels of mitochondrial inner membrane genes in BM1 cells treated with hemin (20 μM) or vehicle and representative protein blots. Three independent experiments repeated with similar results. **b**, Measurement of OCR and ECAR in BM1 cells pre-treated with hemin (20 μM) or vehicle. Mean ± s.e.m., $n = 6$ biologically independent samples, two-tailed *t*-test. **c**, Cell growth, measured as confluence area covered by BM1 cells treated with vehicle, hemin or metformin. **d**, Top, cysteine residues mutated to alanine in haem-binding motifs of BACH1. Bottom, western blots of BACH1 in cell lysates of BM1 and BM1-shBACH1 cells transfected with BACH1(mut) (100 ng) and treated with hemin (10, 20, 40 and 80 μM) for 48 h. Each experiment repeated independently three times with similar results. **e**, Cell growth, measured as confluence area of BM1-shBACH1 cells expressing BACH1(mut), treated with vehicle (veh), hemin (H) or metformin (M). **f**, Relative mRNA levels of mitochondrial genes in shBACH1 cells stably expressing BACH1(mut) and treated with hemin (20 μM) for 48 h. For qRT–PCR analyses in **a**, **f**, mean ± s.e.m., $n = 3$ biologically independent samples, two-tailed *t*-test. For cell growth assays in **c**, **e**, mean ± s.e.m., $n = 6$ biologically independent samples, two-tailed *t*-test. In **c**, **e**, arrow indicates when drugs were added.

pyruvate dehydrogenase (PDH). PDH converts pyruvate to acetyl-coA and is inhibited by pyruvate dehydrogenase kinase (PDK), which phosphorylates PDH on Ser293[23,24] (Fig. 2e). BACH1 knockdown reduces both PDK and PDH Ser293 phosphorylation (pSer293) but not overall PDH levels, thereby up-regulating PDH activity (Fig. 2f and Extended Data Fig. 2e). ChIP assays showed that BACH1 binds to the promoters of PDK genes in BM1 and MB436 but not in BACH1-deficient MB468 cells (Fig. 2g and Extended Data Fig. 2f). By contrast, there was no change in expression of pyruvate carboxylase, which replenishes TCA intermediates by converting pyruvate to oxaloacetate[25] (Extended Data Fig. 2g). These results indicate that BACH1 regulates PDK transcription and PDH phosphorylation, key steps controlling glycolysis and mitochondrial metabolism.

Because loss of BACH1 regulates mitochondrial metabolism, we determined whether BACH1-depleted cells exhibit increased sensitivity to agents that target these pathways. Metformin inhibits mitochondrial ETC complex I as well as other metabolic targets[5,22,26]. Rotenone and antimycin A target ETC complex I and complex III[27], respectively. These inhibitors significantly reduced cell growth and viability in BACH1-depleted cells relative to control cells (Fig. 2h and Extended Data Fig. 3a–c). Cellular resistance to metformin at levels used in previous studies[28,29] reflected the relative expression of BACH1 in MB468 (low), MB436 (intermediate) and BM1 (high) cells (Fig. 1c and Extended Data Fig. 3d, e). As a widely prescribed anti-diabetic drug that can be cytostatic or cytotoxic[5,30], metformin is less toxic than rotenone or antimycin A; we therefore used metformin for further studies (Extended Data Fig. 3f). These results suggest that BACH1 depletion overcomes TNBC resistance to inhibitors of mitochondrial metabolism by increasing dependency on mitochondrial respiration.

Additionally, we added pyruvate (2.5 mM) to BACH1-depleted cells to assess its effect on metformin resistance. Control cells (high BACH1) were resistant to metformin independent of pyruvate, but shBACH1 cells were only resistant to metformin in the presence of pyruvate. The effect of pyruvate on the NAD^+:NADH ratio paralleled metformin resistance (Extended Data Fig. 4a, b), consistent with previous reports[22,26].

The mitochondrial ETC genes induced in BACH1-depleted cells also affected metformin sensitivity. Silencing of *COX15* or *UQCRC1* in BACH1-depleted cells completely restored metformin resistance and rescued cell growth (Extended Data Fig. 4c, d). Notably, neither expression of the metformin transporter (OCT1, encoded by *SLC22A1*)[31] nor mitochondrial biogenesis genes such as peroxisome proliferator-activated receptor gamma (*PPARG*, which encodes PPARγ) or peroxisome proliferator-activated receptor gamma coactivator1-alpha (*PPARGC1A*, which encodes PGC1α)[32] were altered by BACH1 depletion (Extended Data Fig. 4e). These results demonstrate that increased mitochondrial ETC gene expression enhances sensitivity to ETC inhibitor treatment.

As an alternative means of depleting BACH1, we induced BACH1 degradation using hemin, the active ingredient of the FDA-approved drug Panhematin, which is used to treat acute porphyria[33,34]. We treated TNBC cells with a dose that is neither cytotoxic nor inhibits growth, yet is still effective at reducing BACH1 levels (Extended Data Fig. 5a). As observed with shBACH1, hemin increased mitochondrial gene expression and altered cellular metabolic phenotypes, inducing basal and maximum OCR but lowering ECAR (Fig. 3a, b and Extended Data Fig. 5b, c). Similarly, hemin decreased growth and viability of TNBC cells upon treatment with metformin or other ETC inhibitors (Fig. 3c and Extended Data Fig. 5d, e). These results indicate that pharmacological depletion using hemin mimics the phenotype induced by genetic knockdown of BACH1.

To test hemin specificity for BACH1, we generated a haem-resistant mouse BACH1 mutant (BACH1(mut)), which has cysteine to alanine point mutations in four C-terminal haem-binding sites that are required for haem binding, release of BACH1 from DNA for nuclear export and subsequent degradation[7,35] (Fig. 3d and Extended Data Fig. 5f). BACH1(mut), when expressed in shBACH1 TNBC cells, rescues BACH1 function (Extended Data Fig. 5g, h). However, in contrast to control or shRNA-resistant wild-type mouse BACH1, BACH1(mut)-expressing cells were resistant to hemin treatment with respect to metabolic properties and metformin sensitivity (Fig. 3e, f and Extended Data Fig. 5 i–k). These data suggest that hemin acts through specific degradation of BACH1.

We then tested whether BACH1 is a useful therapeutic target in vivo. First, we treated BACH1-depleted xenograft TNBC tumours with metformin in the range commonly used for mouse studies (200–300 mg per kg (body weight))[28,29]. These doses result in mouse tumour and plasma metformin concentrations (3–12 μM) similar to those found in metformin-treated patients with diabetes (~10 μM range)[28,29]. Neither BACH1-depletion nor metformin alone altered tumour size

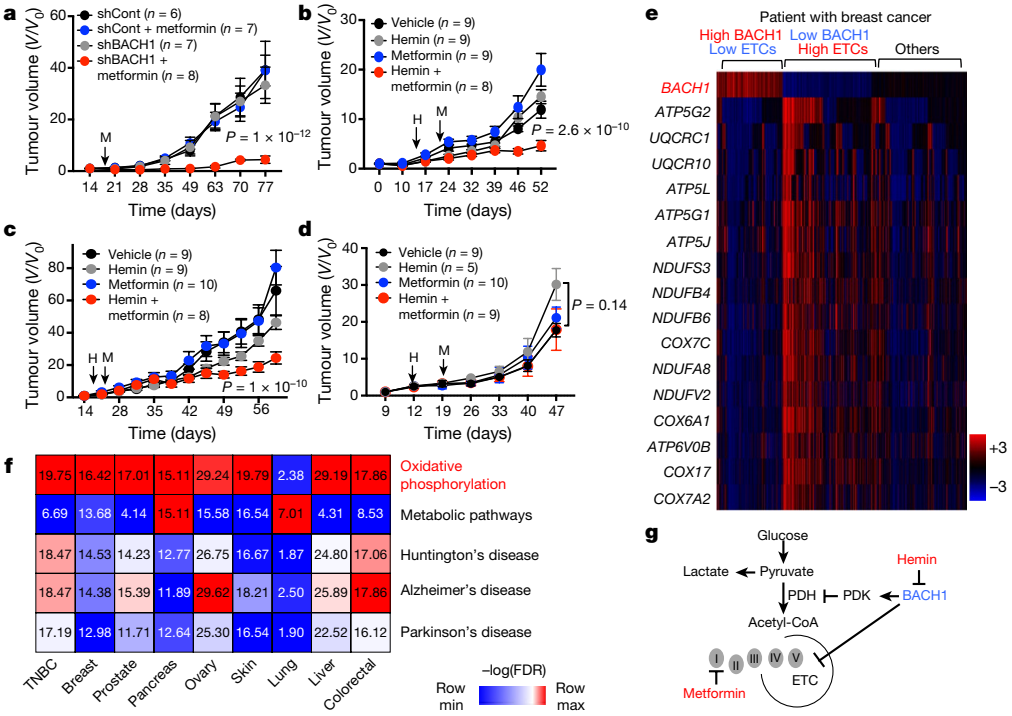

Fig. 4 | Combination treatment with hemin and metformin suppresses tumour growth through BACH1 inhibition. a–d, Relative tumour volumes in athymic nude mice orthotopically injected with MB436-shBACH1 (**a**; shCont $n = 6$, shCont + metformin $n = 7$, shBACH1 $n = 7$, shBACH1 + metformin $n = 8$), MB436 (**b**; vehicle $n = 9$, hemin $n = 9$, metformin $n = 9$, hemin + metformin $n = 8$), PDX (no. 2147) (**c**; vehicle $n = 9$, hemin $n = 9$, metformin $n = 10$, hemin + metformin $n = 8$) and BACH1(mut)-expressing MB436-shBACH1 cells (**d**; vehicle $n = 9$, hemin $n = 5$, metformin $n = 10$, hemin + metformin $n = 9$), treated with hemin (H, 50 mg kg^{-1} day^{-1}) daily by intraperitoneal injection and/or metformin (M, 200 mg per kg (body weight) per day for MB436 xenograft or 300 mg per kg (body weight) per day for BM1 xenograft and PDXs) or vehicle in drinking water ad libitum until end of experiments. Tumour volumes shown relative to initial volume measured before treatment. Mean ± s.e.m., two-tailed *t*-test. **e**, Heat map from OncoPrint analysis demonstrating expression (*z*-scores) of *BACH1* and ETC gene expression for each patient with breast cancer (TCGA provisional dataset, $n = 1105$). *ATP5G2* and *ATP5L* also known as *ATP5MC2* and *ATP5MG*, respectively. **f**, Heat map showing KEGG pathways that are negatively correlated with BACH1 levels across major TCGA cancers such as breast ($n = 1105$), TNBC ($n = 115$), prostate ($n = 497$), pancreas ($n = 186$), ovary ($n = 606$), skin ($n = 472$), lung ($n = 586$), liver ($n = 371$) and colon ($n = 379$). Values shown as −log(FDR) with Benjamini–Hochberg-corrected *P* values (FDR) using the GOseq package. Only KEGG pathways commonly enriched in all cancer types studied are on the heat map. **g**, Proposed model summary of BACH1 regulation of metabolic pathways by inhibiting mitochondrial membrane gene expression and PDH activity; targets of combination therapy by metformin (ETC) and hemin (BACH1) are shown.

compared to control tumours. Notably, metformin suppressed growth of xenograft tumours (BM1 or MB436) that stably express shBACH1, and most grafted mice were tumour-free (Fig. 4a and Extended Data Fig. 6a–c). This reduction in tumours was not a consequence of overall toxicity, as all mice in this and subsequent treatment groups exhibited no change in body weight (Extended Data Fig. 6d). As in cultured cells, the BACH1-depleted tumour cells had low levels of BACH1, reduced PDH pSer293 and increased ETC protein levels (Extended Data Fig. 6e, f). Depletion of BACH1 in MB436 tumours also suppressed lung metastasis, consistent with our previous observations with BM1 cells[10] (Extended Data Fig. 6g, h).

Combination treatment with hemin and metformin also suppressed tumour growth. After tumour formation, we treated BACH1-expressing TNBC cell lines (BM1 and MB436) or patient-derived xenografts (PDX) with hemin for ten days to degrade BACH1 before metformin treatment (Extended Data Fig. 7a–c). Only the combined hemin–metformin treatment significantly suppressed tumour growth (Fig. 4b, c and Extended Data Fig. 7d–f).

Next, to investigate the dependence of combined hemin–metformin treatment on BACH1, we performed BACH1-rescue experiments using BM1 or MB436-shBACH1 cells transfected with mouse BACH1(mut). In contrast to tumours expressing wild-type BACH1, which exhibited reduced growth with hemin–metformin treatment, BACH1(mut) xenograft tumours were resistant to the hemin–metformin treatment (Fig. 4d and Extended Data Fig. 7g–i). Similarly, overexpression of wild-type mouse BACH1 in shBACH1 cells also rescued the resistant phenotype and overcame tumour sensitivity to combined hemin–metformin treatment, which was insufficient to degrade the mouse BACH1 at the dose used (Extended Data Fig. 7j). Taken together, these results show that hemin sensitizes TNBC tumours to metformin by degrading BACH1.

Bioinformatics analyses of clinical samples illustrate the relevance of these findings to patients with cancer. Approximately 40% of TCGA breast tumours express BACH1 at normal or intermediate levels; however, 60% of these tumours express either higher or lower than normal levels of BACH1 (Fig. 4e). Within this subset, BACH1 levels are high in 36% of TNBC samples versus 26% of non-TNBC samples (Extended Data Fig. 8a). Consistent with our preclinical results, BACH1 expression correlates inversely with ETC expression in individual patient tumours (Fig. 4e). Notably, *BACH1* mRNA expression is enriched not only in breast cancer, but also in many other types of cancer including lung, kidney, uterine and prostate cancer, and acute myeloid leukaemia (Extended Data Fig. 8b, c). KEGG analyses of genes that negatively correlate with BACH1 expression in tumours from patients with prostate, pancreas, ovary, skin, liver or colon cancer showed a similar enrichment in oxidative phosphorylation (Fig. 4f and Extended Data Fig. 8d). We also noted inversely correlated expression of BACH1 and ETC genes such as *UQCRC1* in tumours from these other cancer types (Extended Data Figs. 8e, 9a–d). Together, patient data analyses suggest that BACH1 inhibition of mitochondrial ETC genes may be a common mechanism in cancer.

Our results highlight BACH1 as a key regulator of mitochondrial metabolism and a determinant of TNBC response to metformin treatment. The combination of the changes in ETC gene expression,

mitochondrial respiration, levels of both glycolytic and TCA metabolites, and PDK transcription and PDH phosphorylation are consistent with alterations in metabolic pathways and carbon-source use upon BACH1 loss. To our knowledge, the role of BACH1 as a regulator of metabolism has not previously been recognized or studied. Thus, the downstream mechanisms driving the metabolic alterations that we observe upon BACH1 depletion, such as the differences in glutamine and glucose utilization in the TCA cycle, open new areas for investigation. Whereas the targets of BACH1 that we have characterized reflect the most marked changes in enzymes that regulate mitochondrial metabolism, there may be other targets that could potentially affect mitochondrial metabolism in this way.

The marked inverse correlation between *BACH1* and ETC gene expression in individual patients raises the possibility that these biomarkers may be useful for prediction of metformin therapeutic outcome. Our findings also suggest a potential combination therapeutic strategy by repurposing two FDA-approved drugs, hemin and metformin (Fig. 4g). Targeting the BACH1 pathway represents a novel approach to enhance the efficacy of inhibitors of mitochondrial metabolism through restriction of metabolic plasticity. More generally, we propose reprogramming the metabolic network to decrease metabolic variance and increase the fraction of cells with increased dependence on mitochondrial respiration. This approach could also be applied to other tumour types that use BACH1 or other key regulators of mitochondrial metabolism.

Online content

Any methods, additional references, Nature Research reporting summaries, source data, statements of data availability and associated accession codes are available at https://doi.org/10.1038/s41586-019-1005-x.

Received: 25 April 2017; Accepted: 6 February 2019;
Published online 6 March 2019.

1. Vander Heiden, M. G. & DeBerardinis, R. J. Understanding the intersections between metabolism and cancer biology. *Cell* **168**, 657–669 (2017).
2. Weinberg, S. E. & Chandel, N. S. Targeting mitochondria metabolism for cancer therapy. *Nat. Chem. Biol*. **11**, 9–15 (2015).
3. DeBerardinis, R. J. & Chandel, N. S. Fundamentals of cancer metabolism. *Sci. Adv*. **2**, e1600200 (2016).
4. Oyake, T. et al. Bach proteins belong to a novel family of BTB-basic leucine zipper transcription factors that interact with MafK and regulate transcription through the NF-E2 site. *Mol. Cell. Biol*. **16**, 6083–6095 (1996).
5. Wheaton, W. W. et al. Metformin inhibits mitochondrial complex I of cancer cells to reduce tumorigenesis. *eLife* **3**, e02242 (2014).
6. Birsoy, K. et al. Metabolic determinants of cancer cell sensitivity to glucose limitation and biguanides. *Nature* **508**, 108–112 (2014).
7. Ogawa, K. et al. Heme mediates derepression of Maf recognition element through direct binding to transcription repressor Bach1. *EMBO J*. **20**, 2835–2843 (2001).
8. Bianchini, G., Balko, J. M., Mayer, I. A., Sanders, M. E. & Gianni, L. Triple-negative breast cancer: challenges and opportunities of a heterogeneous disease. *Nat. Rev. Clin. Oncol*. **13**, 674–690 (2016).
9. Dangi-Garimella, S. et al. Raf kinase inhibitory protein suppresses a metastasis signalling cascade involving LIN28 and *let-7*. *EMBO J*. **28**, 347–358 (2009).
10. Yun, J. et al. Signalling pathway for RKIP and Let-7 regulates and predicts metastatic breast cancer. *EMBO J*. **30**, 4500–4514 (2011).
11. Lee, U. et al. A prognostic gene signature for metastasis-free survival of triple negative breast cancer patients. *PLoS ONE* **8**, e82125 (2013).
12. Liang, Y. et al. Transcriptional network analysis identifies BACH1 as a master regulator of breast cancer bone metastasis. *J. Biol. Chem*. **287**, 33533–33544 (2012).
13. Sun, J. et al. Hemoprotein Bach1 regulates enhancer availability of heme oxygenase-1 gene. *EMBO J*. **21**, 5216–5224 (2002).
14. Cancer Genome Atlas Network. Comprehensive molecular portraits of human breast tumours. *Nature* **490**, 61–70 (2012).
15. Curtis, C. et al. The genomic and transcriptomic architecture of 2,000 breast tumours reveals novel subgroups. *Nature* **486**, 346–352 (2012).
16. Wang, Y. et al. Gene-expression profiles to predict distant metastasis of lymph-node-negative primary breast cancer. *Lancet* **365**, 671–679 (2005).
17. Schmidt, M. et al. The humoral immune system has a key prognostic impact in node-negative breast cancer. *Cancer Res*. **68**, 5405–5413 (2008).
18. Minn, A. J. et al. Genes that mediate breast cancer metastasis to lung. *Nature* **436**, 518–524 (2005).
19. Igarashi, K. et al. Multivalent DNA binding complex generated by small Maf and Bach1 as a possible biochemical basis for β-globin locus control region complex. *J. Biol. Chem*. **273**, 11783–11790 (1998).
20. Lee, J. et al. Network of mutually repressive metastasis regulators can promote cell heterogeneity and metastatic transitions. *Proc. Natl Acad. Sci. USA* **111**, E364–E373 (2014).
21. Barski, A. et al. High-resolution profiling of histone methylations in the human genome. *Cell* **129**, 823–837 (2007).
22. Liu, X., Romero, I. L., Litchfield, L. M., Lengyel, E. & Locasale, J. W. Metformin targets central carbon metabolism and reveals mitochondrial requirements in human cancers. *Cell Metab*. **24**, 728–739 (2016).
23. Schell, J. C. & Rutter, J. The long and winding road to the mitochondrial pyruvate carrier. *Cancer Metab*. **1**, 6 (2013).
24. Kim, J. W., Tchernyshyov, I., Semenza, G. L. & Dang, C. V. HIF-1-mediated expression of pyruvate dehydrogenase kinase: a metabolic switch required for cellular adaptation to hypoxia. *Cell Metab*. **3**, 177–185 (2006).
25. Jitrapakdee, S., Vidal-Puig, A. & Wallace, J. C. Anaplerotic roles of pyruvate carboxylase in mammalian tissues. *Cell. Mol. Life Sci*. **63**, 843–854 (2006).
26. Gui, D. Y. et al. Environment dictates dependence on mitochondrial complex I for NAD^+ and aspartate production and determines cancer cell sensitivity to metformin. *Cell Metab*. **24**, 716–727 (2016).
27. Murai, M. & Miyoshi, H. Current topics on inhibitors of respiratory complex I. *Biochim. Biophys. Acta Bioenerg*. **1857**, 884–891 (2016).
28. Dowling, R. J. O. et al. Metformin pharmacokinetics in mouse tumors: implications for human therapy. *Cell Metab*. **23**, 567–568 (2016).
29. Chandel, N. S. et al. Are metformin doses used in murine cancer models clinically relevant? *Cell Metab*. **23**, 569–570 (2016).
30. Klil-Drori, A. J., Azoulay, L. & Pollak, M. N. Cancer, obesity, diabetes, and antidiabetic drugs: is the fog clearing? *Nat. Rev. Clin. Oncol*. **14**, 85–99 (2017).
31. Emami Riedmaier, A., Fisel, P., Nies, A. T., Schaeffeler, E. & Schwab, M. Metformin and cancer: from the old medicine cabinet to pharmacological pitfalls and prospects. *Trends Pharmacol. Sci*. **34**, 126–135 (2013).
32. Liang, H. & Ward, W. F. PGC-1α: a key regulator of energy metabolism. *Adv. Physiol. Educ*. **30**, 145–151 (2006).
33. Zenke-Kawasaki, Y. et al. Heme induces ubiquitination and degradation of the transcription factor Bach1. *Mol. Cell. Biol*. **27**, 6962–6971 (2007).
34. Dhar, G. J., Bossenmaier, I., Petryka, Z. J., Cardinal, R. & Watson, C. J. Effects of hematin in hepatic porphyria. Further studies. *Ann. Intern. Med*. **83**, 20–30 (1975).
35. Suzuki, H. et al. Heme regulates gene expression by triggering Crm1-dependent nuclear export of Bach1. *EMBO J*. **23**, 2544–2553 (2004).

Acknowledgements We thank G. Greene and members of his laboratory for sharing the PDX tumors. This study was supported by NIH R01CA184494 (M.R.R.), R01GM121735 (M.R.R.), NIH R01CA172667 (D.K.N.), DoD Breakthrough Breast Cancer BC161588 (J. Lee), NIH 1R01AI131267 (M.G.B.), 1R56ES028149 (M.G.B.) and NIH R01CA193256 (J.W.L.). We also thank G. Balazsi and members of the Rosner laboratory for careful reading of the manuscript.

Reviewer information *Nature* thanks Matthew J. Ellis, Kazuhiko Igarashi and the other anonymous reviewer(s) for their contribution to the peer review of this work.

Author contributions J. Lee and M.R.R. contributed overall experimental design, J. Lee. performed most experiments, A.E.Y. contributed bioinformatics analyses, J.P.W. contributed to BACH1(mut) experiments, C.F. contributed to gene array analyses, P.C.H., C.K. and M.G.B. contributed Seahorse experiments, E.A.G. and D.K.N. contributed mass spectrometry analysis of metabolites, J. Liu, S.M.S. and J.W.L. contributed tracing analysis, J.Y., F.D.R. and P.T. contributed to cell culture or xenograft experiments, M.E. and D.C.R. contributed to PDX experiments, J.A. contributed biostatistics analyses, M.R.R. and J. Lee supervised the project, analysed data and wrote the manuscript with assistance from J.W.L. All authors reviewed the manuscript.

Competing interests The authors declare no competing interests.

Additional information
Extended data is available for this paper at https://doi.org/10.1038/s41586-019-1005-x.
Supplementary information is available for this paper at https://doi.org/10.1038/s41586-019-1005-x.
Reprints and permissions information is available at http://www.nature.com/reprints.
Correspondence and requests for materials should be addressed to M.R.R.
Publisher's note: Springer Nature remains neutral with regard to jurisdictional claims in published maps and institutional affiliations.

METHODS

Cell cultures. Human breast cancer cell lines (MDA-MB-436, MDA-MB-468) and nonmalignant mammary epithelial cells (MCF10A and 184A1) were obtained from ATCC, and BM1 cells were obtained from A. Minn (University of Pennsylvania) and cultured as previously described[9,10,18,20]. Cancer cells were maintained in high-glucose DMEM (25 mM glucose, 4 mM glutamine, without pyruvate) supplemented with 10% FBS (VWR, 89510-085) and penicillin–streptomycin (100 U ml^{-1}, 100 mg ml^{-1}), but cultured in glucose-limited conditions (1–2.5 mM glucose) that mimic tumour microenvironment with 10% FBS and penicillin–streptomycin when treated with inhibitors. Stable knock-down of BACH1 was performed using a lentiviral construct containing shRNA targeting *BACH1* (shBACH1 clone 1: TATGCACAGAAGATTCATAGG; shBACH1 clone 2: ATATCATGGATACAATCCAGC)[10]. Transfected breast cancer cells were selected with puromycin (0.2 μg ml^{-1}) in growth medium for 10 days. Mycoplasma detection was routinely performed to ensure cells were not infected with mycoplasma using MycoAlert Detection kit (Lonza, LT07-218). Cell lines were authenticated by short tandem repeat analysis.

qRT–PCR. Total RNA from cells and tumour samples was isolated using Trizol (Invitrogen) according to the manufacturer's instructions. Two micrograms of total RNA was adapted for qRT–PCR (Applied Biosystem) to generate cDNA. Real-time PCR was carried out using a LightCycler 96 (Roche) and Fast Start Essential DNA master mix (2X) reagent. *Cq* values normalized relative to the expression of endogenous control genes using $2^{(-\Delta\Delta Cq)}$ were plotted. Primer pairs used are shown in Extended Data Table 1.

Cell growth and viability assays. For cell growth assays, breast cancer cells ($5–8 \times 10^3$ cells per well) and non-malignant mammary epithelial cells (8×10^3 cells per well) were plated on 96-well plates to observe growth of cells every 4 h by phase-contrast imaging and shown as per cent confluence of area covered by cells using an IncuCyte Zoom Live Cell Analysis system (Essen Bioscience). After 24 h of plating, inhibitors were added and monitored until control cells reached 100% confluence. One hundred per cent confluence refers to complete coverage of the plates by cells. To determine cell viability, cells were seeded in black-walled 96-well plates overnight and treated with inhibitors. After 48 h, cells were treated with Calcein AM (R&D system) in PBS for 1 h at 37 °C to measure absorbance with excitation at 420 nm and emission at 520 nm using a Victor3 plate reader (PerkinElmer). The absorbance was used to reflect live cell numbers and was normalized to those in control or with vehicles and shown as relative viability (%).

Chemicals. Hemin (Sigma, H9039 and 51280) was prepared in 20 mM NaOH for in vitro assays or further diluted in PBS (1:5) to adjust pH 7.5 and filter-sterilized using 0.22-μm filters for mouse treatments. Rotenone (Sigma, R8875), antimycin A (Sigma, A8674) and metformin hydrochloride (Sigma, PHR1804) were prepared as stock solutions and added to growth medium. Sodium pyruvate (Gibco, 11360), D-glucose (Sigma, G8769) or L-glutamine (Invitrogen, 25030081) was added to growth medium and filter-sterilized before use. D-Glucose (U-$13C_6$, 99%) and L-Glutamine ($13C_5$, 99%) were purchased from Cambridge Isotope Laboratories.

siRNA. siRNAs for *UQCRC1* (Human *UQCRC1* Flexi tube siRNA, SI00051275, Qiagen, CCGGACAATGTGGCCTTGCAA), *COX15* (Human *COX15* Flexi Tube siRNA, SI014180911, Qiagen, TCCGCCGTTGAGGGCCTTGAA) or siRNA control (Universal Scrambled negative control siRNA, SR30004, Origen, UGGUUUACAUGUCGACUAA, UGGUUUACAUGUUGUGUGA,UGGUUUACAUGUUUUCUGA,UGGUUUA CAUGUUUUCCUA) were transfected into breast cancer cells with Lipofectamine 3000 (Invitrogen) in OPTI-MEM overnight for in vitro assays.

Mutant *Bach1*. Mutant *Bach1* was synthesized with Cys to Ala mutations at haem-binding residues Cys438, Cys464, Cys495 and Cys649 (Thermo Fisher), cloned into pCDNA3.1 and sequenced for mammalian cell transduction using Lipofectamine 3000 (Invitrogen). For stably expressing mouse BACH1(mut) or wild-type BACH1 in BM1-shBACH1 and MB436-shBACH1 cell lines, $Bach1^{mut}$ and $Bach1^{WT}$ sequences were cloned into pCDH for lentiviral transfection.

ChIP assays. Two million cells were plated on 10-cm plates overnight before crosslinking with 10% formaldehyde for 10 min followed by quenching with glycine (0.125 mM) for 3 min. After washing cells with cold PBS, total cell lysates in ice were sonicated at 80% output for 10 s with a 10-s pause for 4 cycles and pre-cleared with IgG (Santa Cruz, sc-2028) for 1 h at 4 °C. Supernatants were precipitated with antibodies against BACH1 (AF5776, R&D System), RNA Pol II phosphoS5 (Abcam, ab5131), histone H3 tri methyl K27 (Abcam, ab6002) or IgG (normal mouse IgG, Santa Cruz, sc-2025) overnight at 4 °C and washed for PCR as previously described[20]. Primers for ChIP-PCR are shown in Extended Data Table 1.

Immunoblotting. Whole-cell or tumour lysates were prepared using RIPA buffer (Sigma, R2078) with protease inhibitor cocktail set III (Millipore, 539134) and phosphatase inhibitors (SimpleStop1, Gold Biotechnology) at 4 °C and quantified using Bradford assays before blotting using antibodies for BACH1 (sc-271211, Santa Cruz), PDK1 (C47H1) (Cell Signaling, no. 3820), PDH (Cell Signaling, #2784), PDH [p-Ser293] (Novusbio, BB110-93479), ATP5D (Abcam, ab107077), SLC25A15 (Novus Biologicals, NBP2-20387), UQCRC1 (Abcam, ab118687), COX15 (Sigma, av46442-100UL), NDUFA9 (Abcam, ab14713), and α-tubulin (Santa Cruz, sc-28199). Blots were imaged, processed and quantified using a Licor Odyssey Fc, dual-mode imaging system (Licor).

NAD^+/NADH. NAD(H) was measured using the NAD^+/NADH-Glo Assay kit (Promega, G9071) in accordance with the manufacturer's protocol.

Metabolic phenotypes. ECAR and OCR were monitored using a Seahorse Bioscience Analyzer (XF24; University of Illinois at Chicago and XFe96; Biophysics Core Facility at University of Chicago) according to the manufacturer's instructions. Cells were seeded in 24-well plates at a density of 5×10^4 and 96-well plates at a density of $5–8 \times 10^3$ cells per well with growth medium for at least 18 h. The following day, medium was changed to base medium (DMEM, 143 mM NaCl, phenol red, pH 7.35). For ECAR analysis, cells were added with medium (2 mM glutamine, pH 7.35) and monitored every 3 min following successive administration of 10 mM of glucose, and inhibitors (1 μM oligomycin and 50 mM 2-deoxyglucose). For OCR analysis, cells were added with mito stress-test base medium (10 mM glucose, 2 mM glutamine, 1 mM pyruvate, pH 7.4) and monitored every 3 min following successive administration of inhibitors (2 μM oligomycin, 2 μM FCCP, or 0.5 μM rotenone/antimycinA). BCA protein assays were used to normalize metabolic rates to cell number.

Lung metastasis. Whole fixed lungs were evaluated by serial sectioning every 100 μm and followed by haematoxylin and eosin (H & E) staining (Human Tissue Resource Center, University of Chicago) for visualization of lung metastases under a microscope (Evos XL cell imaging system, Thermo Fisher).

Mouse experiments. All animal protocols related to mouse experiments were approved by the University of Chicago Institutional Animal Care and Use Committee (IACUC #72228). No statistical methods were used to predetermine sample size. The experiments were not blinded to allocation during experiments and outcome assessment. Two million human breast cancer cells (MDA-MB-436, MDA-MB436-shCont, MDA-MB436-shBACH1, BM1-shCont, BM1-shBACH1, BM1-shBACH1+ BACH1(mut), BM1-shBACH1+ BACH1(WT)) in 100 μl PBS were injected into the fourth mammary fat pad of 5 to 6 week-old athymic nude female mice (Charles River Laboratories). When tumours reach about 20–30 mm^3 in volume, mice were randomized into groups for treatment with hemin (50 mg kg^{-1} day^{-1}) or vehicle (20 mM NaOH in phosphate buffered saline) by intraperitoneal injection 10 days before metformin treatment. Metformin (200 mg kg^{-1} day^{-1} for MB436 xenograft; 300 mg kg^{-1} $day^{-1}$for BM1 xenograft and PDX mice) was provided in drinking water ad libitum.

For BACH1-expressing TNBC PDX models, frozen PDX tumours (no. 2147 and no. 4195)[36] in 0.5 ml of sterile HBSS were prepared in a volume of 10–20 mm^3. In brief, tumour fragments were implanted into the mammary fat pads of five-week-old SCID-beige mice following standard procedures. When tumours reached 50 mm^3 in volume, hemin (50 mg kg^{-1} day^{-1}, intraperitoneal injection) and metformin (300 mg kg^{-1} day^{-1}) in drinking water were administered until the end of experiment. Tumour growth was monitored weekly by caliper measurement in two dimensions to generate ellipsoid volumes using the equation of volume $= 0.4 \times (\text{length} \times \text{width}^2)$. Tumour weight was measured at the end of drug treatment in all mouse experiments. Tumour size (volume and weight) was shown as mean ± s.e.m. with *P* values determined by two-tailed *t*-test or two-way ANOVA with multiple comparisons. Experimental end point was reached when tumour growth reached 2 cm in diameter. Body weights of all mice were monitored regularly before and after treatment. Mouse experiments were performed one time per tumour model.

Statistics. Gene expression in patient data, qRT–PCR, ChIP assays, viability assays, metabolomics, tracing analyses and tumour sizes were analysed to compare values measured in control groups relative to shBACH1 or hemin-treated cells by two-tailed student's *t*-test using GraphPad Prism v.7.0a software. In vitro experiments were independently repeated at least three times for statistical analyses. For ChIP assays, at least three independent biological replicates were used for relative enrichment of BACH1 on the designated promoter regions compared to IgG enrichment. For viability assays, at least six biological replicates of shBACH1 or hemin-treated cells were analysed to compare to shRNA control cells or vehicle-treated cells (shown 100%), respectively. For assays involving cell growth using IncuCyte Zoom or metabolic phenotype using Seahorse, *P* values were determined by paired two-tailed *t*-test. For co-expression analyses using data from patients with cancer, Pearson's and Spearman's correlation coefficients were used. For in vivo mouse experiments, at least five mice were used for each experimental group. Mouse allocation to treatment groups was randomized when tumours reached palpable minimum size, and mice that failed tumour formation were excluded from the experiments. No blinding was done for drug treatment or tumour measurement. All the statistical analyses were validated by the Center for Research Informatics (CRI) at University of Chicago.

Gene set analysis and gene set enrichment analysis. The R package GSA[37] was used to determine which gene sets were enriched in the shBACH1 phenotype.

Two hundred permutations were used to estimate FDR. Enriched gene sets with FDR-corrected *P* values higher than 5% were filtered out. After the initial enrichment analysis, positively correlated (enrichment score >0) and negatively correlated (enrichment score <0) were considered separately.

Gene set enrichment analysis (GSEA) was conducted on the desktop version of the GSEA software (v.2.2.3). The 'max-probe' option was used for collapsing expression values of genes with multiple probes. Gene-set size was limited to an arbitrary cut-off of up to 500 genes per set, and genes were ranked by significance as defined by FDR-corrected *P* value <5%. As above, 200 permutations were used to estimate FDR for GSEA analysis.

Analysis of data from patients with breast cancer. For TCGA, BACH1 expression data (RNA Seq V2 RSEM) from 817 publicly available cases of breast cancer were downloaded from the cBioPortal website[38,39] (https://www.cbioportal.org, accessed February 2017) in the form of *z*-score-transformed data. The clinical data associated with these breast cancer cases were also downloaded from the same website. The TNBC subpopulation within the breast cancer cases was determined by 'negative' status for the immunohistochemistry scores of *ER* (also known as *ESR1*), *PR* (also known as *PGR*) and *HER2* (also known as *ERBB2*) genes (total of 83 cases). For the analysis of BACH1 expression across different Pam50 categories, TCGA breast cancer expression and clinical data were accessed and processed using the R package TCGAbiolinks[40] (installed through https://www.bioconductor.org). This analysis was done solely on cases for which Pam50 classification information was available (total of 522 cases: 98 basal, 58 HER2-enriched, 231 luminal-A, 127 luminal-B and 8 normal-like). Statistical significance of differential BACH1 expression between different Pam50 subgroups, as well as TNBC versus non-TNBC, were determined by two-tailed Student's *t*-test.

Comparison of BACH1 expression levels in different cancer types was conducted on the basis of expression values ($\log_2$) obtained by RNA-sequencing analysis (RNA-seq) of BACH1 in the provisional TCGA datasets. All cases (complete and incomplete) were used for each cancer type. Genes that are negatively correlated with BACH1 were determined based on a Spearman coefficient cut-off of ± 0.3. These selected genes were then subjected to KEGG pathway-enrichment analysis either by over-represented DAVID (https://david.ncifcrf.gov/home.jsp) using Benjamini-corrected *P* value (FDR) or by the R package GOseq[41] using the default program of Wallenius *P* value with Benjamini–Hochberg-corrected *P* values (https://bioconductor.org/packages/release/bioc/html/goseq.html).

The frequency of tumours that have upregulated BACH1 expression with respect to their matched healthy tissue was determined using the online tool BioXpress[42] (https://hive.biochemistry.gwu.edu/bioxpress). Only those TCGA samples that have matched normal tissue expression data were used for this analysis.

For METABRIC, GSE2023 and GSE11121 datasets, the Breast Cancer Integrative Platform processed with uniform normalization methods was accessed for BACH1 analysis at https://omics.bmi.ac.cn/bcancer/ (accessed July 2017)[43].

Metabolomics profiling. As previously reported with metabolomics profiling, BACH1-depleted BM1 and control cells (2×10^6 cells) were cultured in 10-cm dishes with DMEM (10 mM glucose, 4 mM glutamine, 10% FBS) for 16 h and serum-starved for 2 h. Cells were washed with PBS three times, collected in 1 ml PBS per replicate, and flash-frozen[44]. For polar metabolites, cell pellets were extracted in a 40:40:20 mix of acetonitrile:methanol:water including 10 nM D3-^{15}N-serine (CIL) as an internal standard. Insoluble debris was separated by centrifugation at 13,000 r.p.m. for 10 min. Aliquots of extracts were then injected into an Agilent 6460 or 6430 QQQ-liquid chromatography–tandem mass spectrometry (LC–MS/MS) instrument. Separation of metabolites was achieved using normal-phase chromatography with a Luna 5-mm NH_2 column (Phenomenex) using a mobile phase (buffer A, acetonitrile, followed by buffer B, 95:5 water:acetonitrile) with the modifiers 0.1% formic acid or 0.2% ammonium hydroxide/50 mM ammonium acetate for positive and negative ionization mode, respectively. Each run used the same flow: 100% A at 0.2 ml min^{-1} for 5 min, followed by a gradient starting at 0% B and linearly increasing to 100% B in 15 min with a flow rate of 0.7 ml min^{-1}, succeeded by an isocratic gradient of 100% B for 5 min at 0.7 ml min^{-1} before equilibrating for 5 min with 0% B at 0.7 ml min^{-1}.

For non-polar metabolites, cell pellets were extracted in 3 ml chloroform: methanol (2:1) and 1 ml PBS along with internal standards dodecylglycerol (10 nmol, Santa Cruz Biotechnology) and pentadecanoic acid (10 nmol, Sigma-Aldrich). Organic and aqueous layers were separated via centrifugation (1,000*g* for 5 min) and the organic layer collected, dried under nitrogen and dissolved in 120 µl chloroform. For nonpolar metabolites, metabolomes were separated using reverse-phase chromatography with a Luna C5 column (50 mm × 4.6 mm with 5-µm-diameter particles, Phenomenex). Mobile phase A was 95:5 water:methanol and mobile phase B was 60:35:5 ratio of 2-propanol: methanol: water. The positive-ionization mode uses 0.1% formic acid and 5 mM ammonium formate. The negative mode uses 0.1% ammonium hydroxide. The flow rate started at 0.1 ml min^{-1} for 5 min to alleviate backpressure associated with injecting chloroform. The gradient began at 0% B and increased linearly to 100% B over the course of 45 min at a flow rate of 0.4 ml min^{-1}, followed by an isocratic gradient of 100% B for 17 min at 0.5 ml min^{-1} before equilibrating for 8 min at 0% B with a flow rate of 0.5 ml min^{-1}.

Mass spectrometry analysis was performed with an electrospray ionization source on an Agilent 6430 or 6460 QQQ LC–MS/MS (Agilent Technologies). The capillary voltage was set to 3.0 kV, and the fragmentor voltage to 100 V. The drying gas temperature was 350 °C, flow rate was 10 l min^{-1}, and nebulizer pressure was 35 psi. Metabolites were identified by selected reaction monitoring of the transition from precursor to product ions at associated optimized collision energies and retention times as previously described[45]. Metabolites were quantified by integrating the area under the curve, and then normalized to internal standard values.

^{13}C metabolic tracer analyses. To monitor incorporation of ^{13}C into metabolites, BACH1-depleted BM1 and control cells (2×10^5 cells per well) in six-well plates were cultured in DMEM containing 10 mM of uniformly labelled $^{13}C_6$ glucose (4 mM ^{12}C glutamine), 4 mM uniformly labelled $^{13}C_5$ glutamine (10 mM ^{12}C glucose), or 10 mM ^{12}C glucose and 4 mM ^{12}C glutamine for 16 h and harvested in 80% methanol in water on dry ice. After a freeze–thaw cycle at −80 °C, cell supernatants were collected by centrifugation at 20,000*g* for 10 min and dried using a speed vac for 3 h for the further liquid chromatography–mass spectrometry (LC–MS) analysis. ^{13}C metabolic tracer analyses were performed as previously described[46,47].

Reporting summary. Further information on research design is available in the Nature Research Reporting Summary linked to this paper.

Data availability

All data are available from the authors upon reasonable request. Additional material including source data is available online.

36. Zhang, X. et al. A renewable tissue resource of phenotypically stable, biologically and ethnically diverse, patient-derived human breast cancer xenograft models. *Cancer Res.* **73**, 4885–4897 (2013) .
37. Efron, B. & Tibshirani, R. On testing the significance of sets of genes. *Ann. Appl. Stat.* **1**, 107–129 (2007).
38. Cerami, E. et al. The cBio cancer genomics portal: an open platform for exploring multidimensional cancer genomics data. *Cancer Discov.* **2**, 401–404 (2012).
39. Gao, J. et al. Integrative analysis of complex cancer genomics and clinical profiles using the cBioPortal. *Sci. Signal.* **6**, pl1 (2013).
40. Colaprico, A. et al. TCGAbiolinks: an R/Bioconductor package for integrative analysis of TCGA data. *Nucleic Acids Res.* **44**, e71 (2016).
41. Young, M. D., Wakefield, M. J., Smyth, G. K. & Oshlack, A. Gene ontology analysis for RNA-seq: accounting for selection bias. *Genome Biol.* **11**, R14 (2010).
42. Wan, Q. et al. BioXpress: an integrated RNA-seq-derived gene expression database for pan-cancer analysis. *Database* **2015**, bav019 (2015).
43. Wu, J. et al. BCIP: a gene-centered platform for identifying potential regulatory genes in breast cancer. *Sci. Rep.* **7**, 45235 (2017).
44. Louie, S. M. et al. GSTP1 Is a driver of triple-negative breast cancer cell metabolism and pathogenicity. *Cell Chem. Biol.* **23**, 567–578 (2016).
45. Benjamin, D. I. et al. Ether lipid generating enzyme AGPS alters the balance of structural and signaling lipids to fuel cancer pathogenicity. *Proc. Natl Acad. Sci. USA* **110**, 14912–14917 (2013).
46. Gao, X. et al. Serine availability influences mitochondrial dynamics and function through lipid metabolism. *Cell Reports* **22**, 3507–3520 (2018).
47. Liu, J. & Locasale, J. W. Metabolomics: A primer. *Trends Biochem. Sci.* **42**, 274–284 (2017).

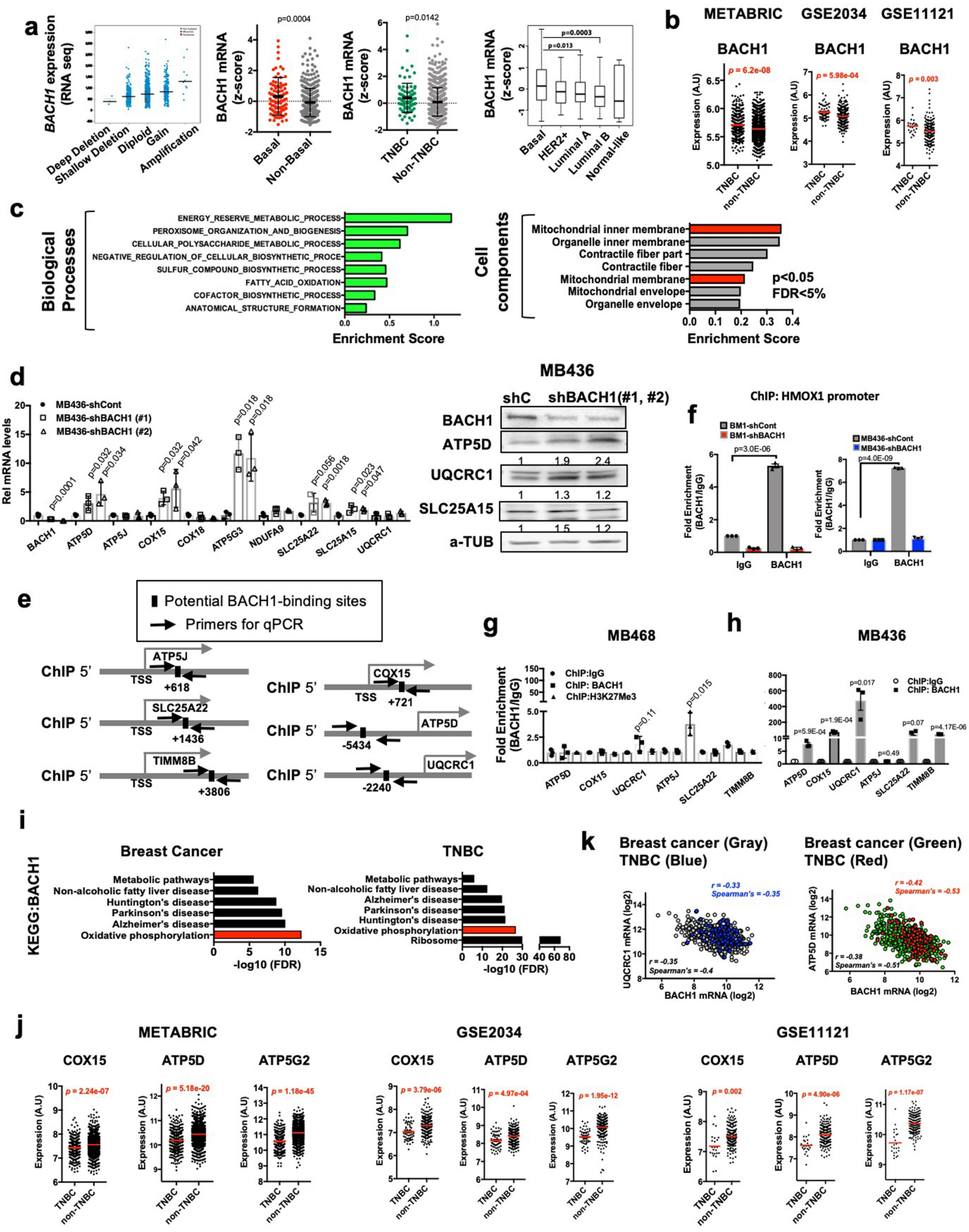

Extended Data Fig. 1 | See next page for caption.

Extended Data Fig. 1 | BACH1 expression is high in patients with TNBC and suppresses expression of ETC genes at their promoter. **a**, Left, BACH1 expression levels (determined by RNA-seq) with respect to relative DNA copy-number alterations in TCGA breast cancers ($n = 1105$). Middle, *BACH1* expression (RNA-seq) in TNBC ($n = 83$) or basal ($n = 98$) breast cancers compared to non-TNBC ($n = 734$) or non-basal ($n = 424$) breast cancers using Pam50 classification of TCGA data. Right, breast cancer subtypes classified by Pam50 ($n = 522$ total, $n = 98$ basal, $n = 58$ *HER2*-enriched, $n = 231$ luminal-A, $n = 127$ luminal-B, $n = 8$ normal-like). Two-tailed *t*-test. **b**, BACH1 expression levels (by RNA-seq) in patients with TNBC compared to patients that did not have TNBC, using the datasets of patients with breast cancer of METABRIC ($n = 2509$), GSE2034 ($n = 286$) and GSE11121 ($n = 200$). Two-tailed *t*-test. **c**, Gene Ontology terms as determined by gene set analysis for cell components that are positively correlated with BACH1 depletion based on microarray analysis of BM1-shBACH1 cell transcripts. $n = 3$ biologically independent samples, FDR-corrected $P < 0.05$. **d**, Left, relative mRNA levels of mitochondrial inner membrane genes in MB436-shBACH1 cells (two shBACH1 vectors, clone 1, clone 2) compared to the wild type control (MB436-shCont). Data are mean ± s.e.m., $n = 3$ biologically independent samples, two-tailed *t*-test. Right, representative western blots of mitochondrial genes using MB436-shBACH1 or control cell lysates. Each experiment was repeated independently three times with similar results. Band density quantification is shown below the blots. **e**, Schematic showing proximal BACH1 binding on the promoter regions of mitochondrial membrane genes. TSS, transcription start site. Arrows, primers used for ChIP-PCR. **f**, ChIP assays showing relative fold enrichment of BACH1 recruitment to the *HMOX1* promoter using BACH1-depleted TNBC (BM1 and MB436) or control cells. **g**, **h**, ChIP assays showing fold enrichment of BACH1 and H3K27me3 recruitment to the mitochondrial membrane genes in low-BACH1-expressing MB468 and MB436 cells. For ChIP assays in **f**–**h**, data are mean ± s.e.m., $n = 3$ biologically independent samples, two-tailed *t*-test. **i**, KEGG pathways demonstrating the negative correlation between BACH1 expression and oxidative phosphorylation in all patients with breast cancer ($n = 1{,}105$, left) and patients with TNBC ($n = 119$, right). FDR values ($-\log_{10}$(FDR)) are generated in the R package GOseq using the default program Wallenius *P* values with Benjamini−Hochberg-corrected *P* values. **j**, Expression of ETC genes (*COX15*, *ATP5D* and *ATP5G2* (also known as *ATP5MC2*)) in TNBC compared to tumours from patients that did not have TNBC using multiple breast cancer datasets: METABRIC (TNBC $n = 319$, non-TNBC $n = 1661$), GSE2034 (TNBC $n = 54$, no*n*-TNBC $n = 232$) and GSE11121 (TNBC $n = 33$, no*n*-TNBC $n = 150$). *P* values are determined by two-tailed *t*-test. **k**, Co-expression plots of UQCRC1 or ATP5D and BACH1 in TCGA breast cancer ($n = 1105$) or TNBC ($n = 115$) dataset. Pearson's and Spearman's correlation coefficients are shown.

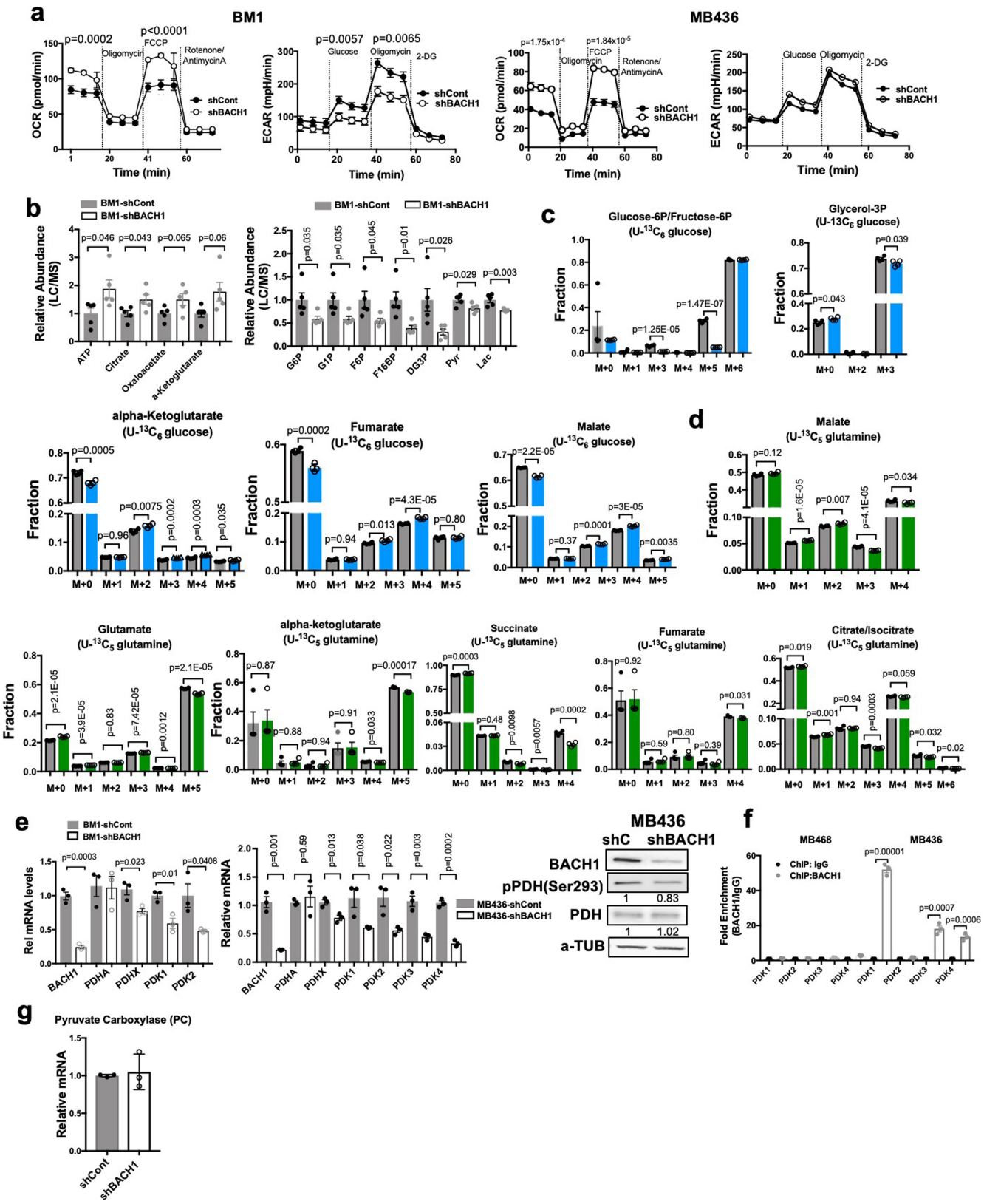

Extended Data Fig. 2 | See next page for caption.

Extended Data Fig. 2 | BACH1 depletion increases mitochondrial metabolism. a, Measurement of OCR and ECAR in BM1 or MB436 cells expressing control or shBACH1. Data are mean ± s.e.m., $n = 6$ biologically independent samples, unpaired two-tailed *t*-test. **b**, Relative abundance of steady-state metabolites in BM1-shBACH1 or control cells cultured with DMEM (glucose, 10 mM) measured by mass spectrometry. Pyr, pyruvate; Lac, lactate. Data are mean ± s.e.m., $n = 5$ biologically independent samples, two-tailed *t*-test. **c**, **d**, Fractional isotopic incorporation of [U-$^{13}C_6$]-glucose (**c**) or [U-$^{13}C_5$]-glutamine (**d**) into the metabolites in glycolysis and the TCA cycle are shown. Data are mean ± s.e.m., $n = 4$ biologically independent samples, two-tailed *t*-test. *M* indicates number of carbons labelled. Fraction is ratio of isotopologues to sum of all isotopologues. **e**, Relative mRNA and protein levels of PDH and PDK genes in MB436-shBACH1 cells compared to controls. qRT–PCR data are mean ± s.e.m., $n = 3$ biologically independent samples, two-tailed *t*-test. Representative images of western blots are shown. Band density quantification is shown below the blots. Each experiment was repeated independently three times with similar results. **f**, ChIP assays showing fold enrichment of BACH1 recruitment to promoters of PDK genes using MB436 and MB468 cells. Data are mean ± s.e.m., $n = 3$ biological replicates per cell line, two-tailed *t*-test. **g**, Relative mRNA levels of pyruvate carboxylase (*PC*) in shBACH1 cells compared to control. Data are mean ± s.e.m., $n = 3$ biologically independent samples. NS, not significant by two-tailed student's *t*-test.

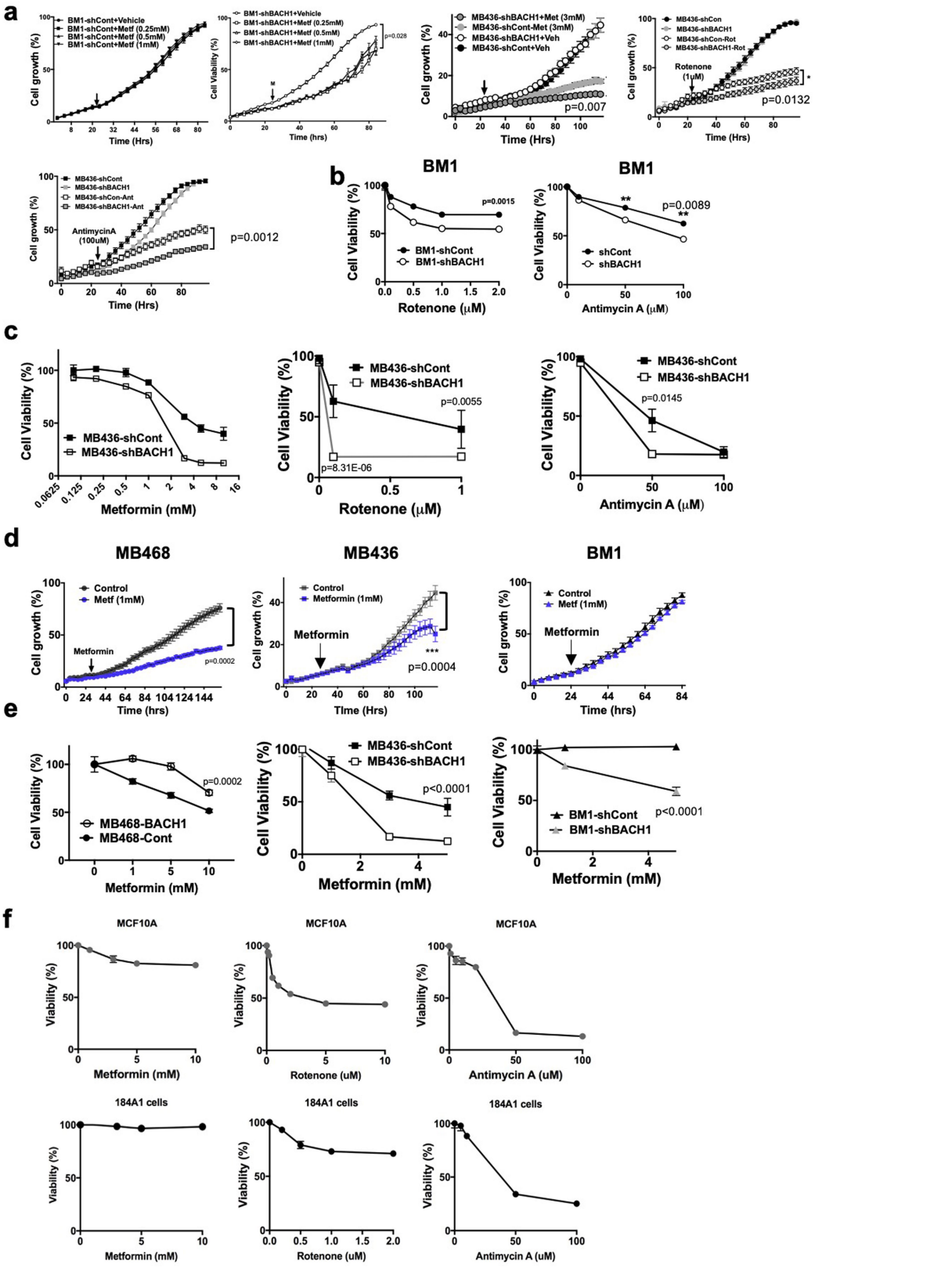

Extended Data Fig. 3 | BACH1 levels determine response to ETC inhibitor treatment in breast cancer cells. a, Cellular growth (per cent confluency) of BACH1-depleted cells (BM1-shBACH1 or MB436-shBACH1) or their controls treated with vehicle (veh), metformin (met), rotenone (rot) or antimycin A (ant). **b**, **c**, Relative cell viability (%) of BACH1-depleted cells (BM1-shBACH1 or MB436-shBACH1) or their controls treated with vehicle, metformin, rotenone or antimycin A. **d**, **e**, Cellular growth (per cent confluency) (**d**) or cell viability (%) (**e**) of low-BACH1 (MB468), medium-BACH1 (MB436) or high-BACH1 (BM1)-expressing TNBC cells treated with vehicle (control), 1 mM metformin, or 1–10 mM metformin. **f**, Cell viability (%) of non-malignant mammary epithelial cells (MCF10A and 184A1) treated with vehicle, metformin, rotenone or antimycin A. For cell viability and growth assays in **a** and **d**, values are mean ± s.e.m., $n = 6$ biologically independent samples, unpaired two-tailed t-test. Arrow indicates the time at which inhibitors were added. For cell viability assays in **b**, **c**, **e** and **f**, cells were incubated for 48 h after addition of inhibitors and stained with CaAM for 1 h.

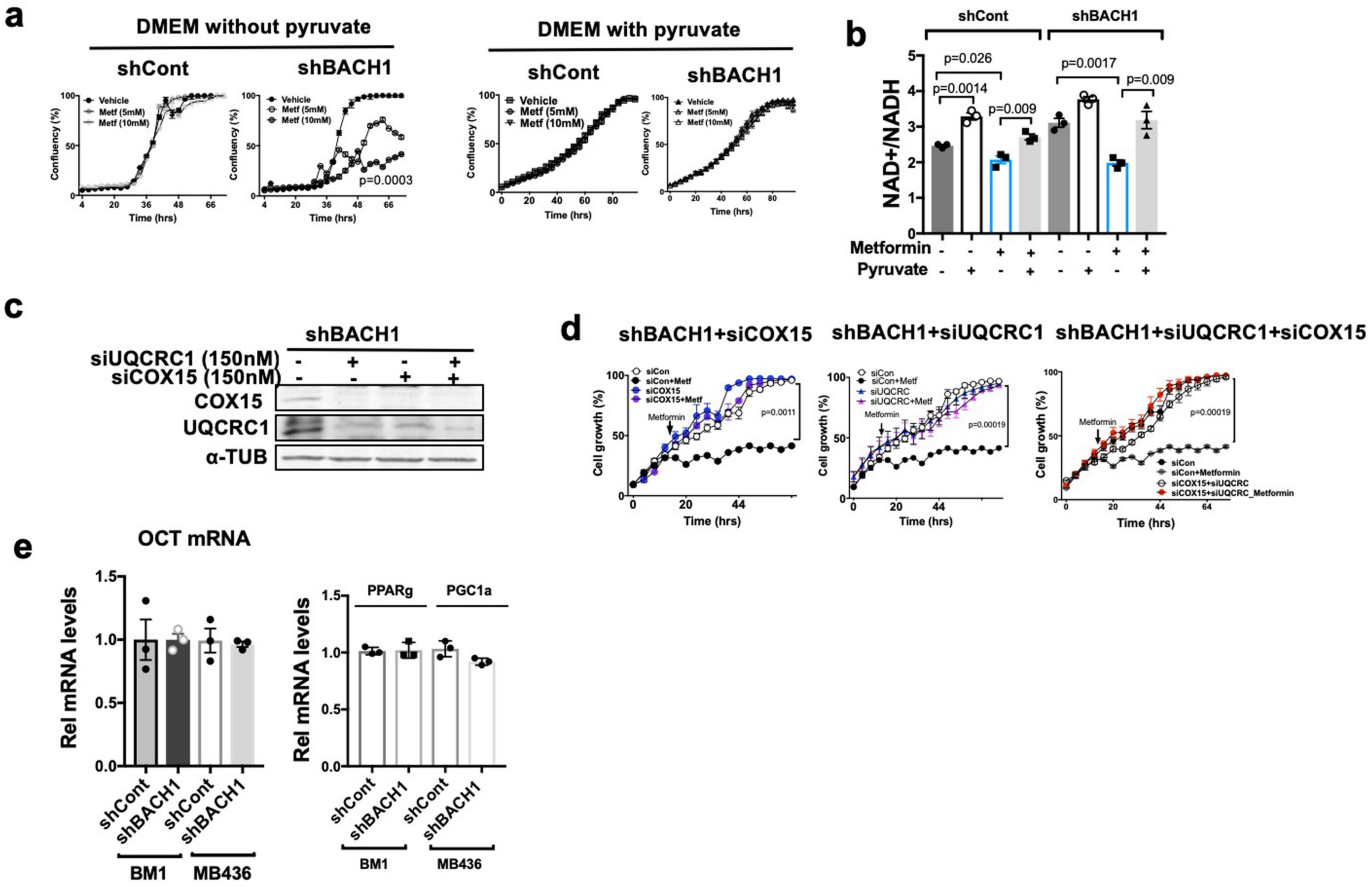

Extended Data Fig. 4 | Rescue of BACH1-depleted TNBC cells from metformin treatment. a, Cellular growth (per cent confluency) of BM1-shBACH1 or control cells treated with vehicle or metformin in growth medium containing glucose (1 mM) and supplemented with or without pyruvate (2.5 mM). **b**, Relative NAD^+/NADH ratios in BACH1-depleted BM1 cells treated with pyruvate (2.5 mM) and/or metformin (5 mM) for 24 h. Data are mean ± s.e.m., $n = 3$ biologically independent samples, two-tailed *t*-test. **c**, Representative western blots of COX15, UQCRC1 and α-tubulin using BM1-shBACH1 cell lysates transfected with siCOX15 (150 nM), siUQCRC1 (150 nM), and siControl (150 nM). Each experiment was repeated independently two times with similar results. **d**, Cellular growth (per cent confluence) of BM1-shBACH1 cells transfected with siRNA for *COX15* and/or *UQCRC1* and treated with vehicle or metformin (10 mM). For **a** and **d**, data are mean ± s.e.m., $n = 6$ biologically independent samples, unpaired two-tailed *t*-test between vehicle-treated and metformin (10 mM)-treated group. **e**, Relative *OCT1* (also known as *SLC22A1*, left), *PPARG* and *PGC1A* (also known as *PPARGC1A*, right) mRNA levels in BM1-shBACH1 cells. Data are mean ± s.e.m., $n = 3$ biologically independent samples.

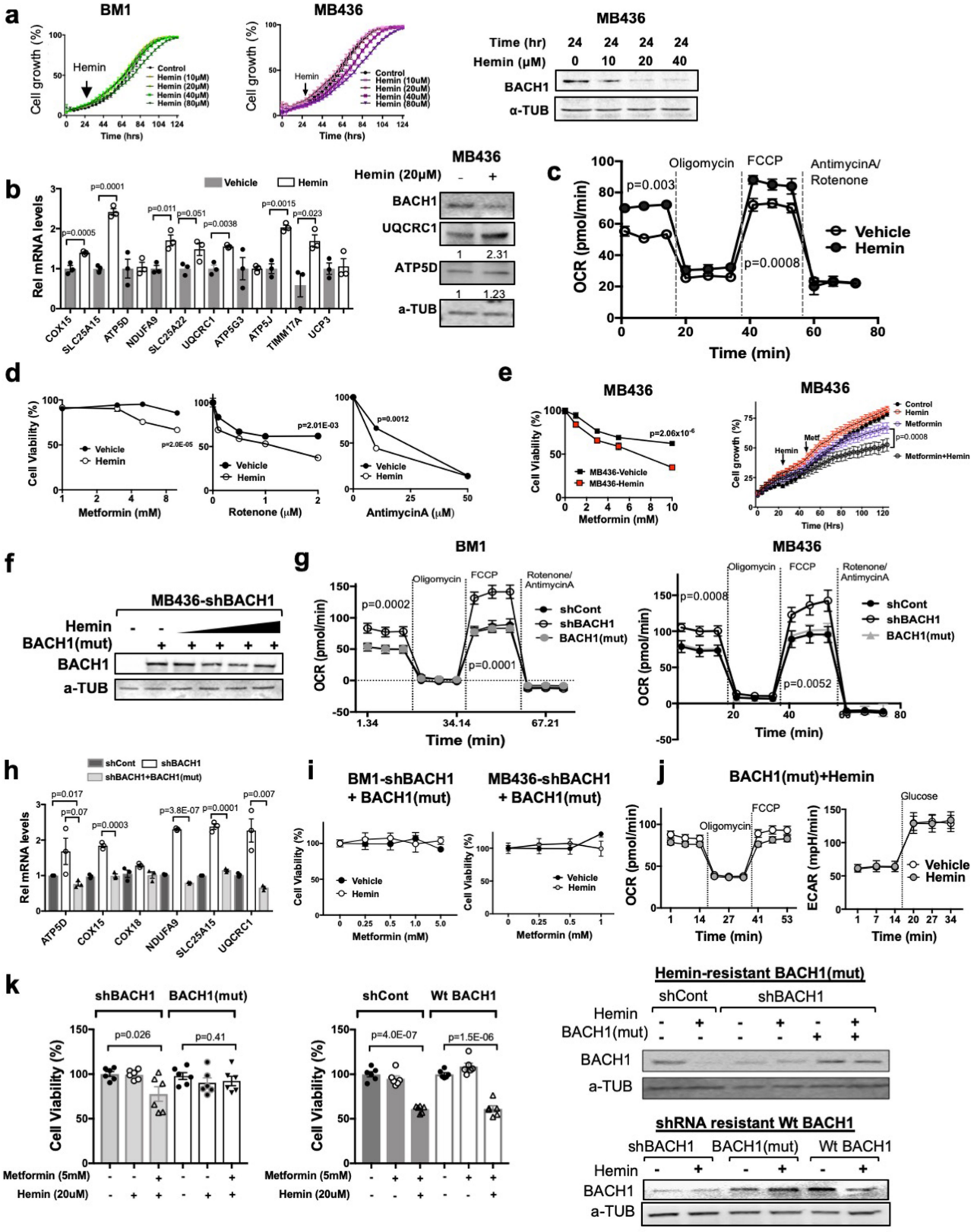

Extended Data Fig. 5 | See next page for caption.

Extended Data Fig. 5 | Hemin treatment of cells expressing wild-type BACH1 or hemin-resistant BACH1(mut). a, Left, cellular growth (per cent confluence) of BM1 and MB436 cells treated with hemin (10, 20, 40 or 80 μM) as indicated. Right, representative western blots of BACH1 from MB436 cells after treatment with hemin (10–40 μM) for 24 h (see also Fig. 3d). Each experiment was repeated independently three times with similar results. **b**, Relative mRNA levels of mitochondrial membrane genes in MB436 cells treated with vehicle or hemin (20 μM) for 48 h. and representative western blots. Data are mean ± s.e.m., $n = 3$ biologically independent samples, two-tailed *t*-test. Band density quantification is shown below the blots. **c**, Measurement of OCR or ECAR of BM1 cells treated with vehicle or hemin (full data from Fig. 3b). **d**, Cell viability (%) of BM1 cells treated with vehicle, hemin (20 μM) or ETC inhibitors (metformin, rotenone or antimycin A) for 48 h. **e**, Cell viability (%) or cell growth (per cent confluence) of MB436 cells treated with vehicle, hemin (20 μM) or metformin (1 mM). **f**, Representative western blots from MB436-shBACH1 cells transiently transfected with *Bach1*^{mut} (100 ng) and treated with vehicle or hemin (10, 20, 40 or 80 μM) for 48 h. Each experiment was repeated independently three times with similar results. **g**, Measurement of OCR in BM1 or MB436 cells stably expressing shControl, shBACH1 or shBACH1 + *Bach1*^{mut} vectors. **h**, Relative mRNA levels of mitochondrial genes in BM1-shBACH1 cells, shCont cells, or BM1-shBACH1 cells transfected with BACH1(mut). Data are mean ± s.e.m., $n = 3$ biologically independent samples, two-tailed *t*-test. **i**, Left, cell viability (%) of BM1-shBACH1 cells transfected with BACH1(mut) and then treated with hemin (20 μM) or vehicle for 48 h. Right, representative western blots showing BACH1(mut) from cells treated with vehicle or hemin. **j**, Measurement of OCR and ECAR of BM1-shBACH1 cells expressing BACH1(mut) pre-treated with hemin. Conditions for OCR and ECAR, and statistics are the same as in Extended Data Fig. 2a. Data are mean ± s.e.m., $n = 6$ biologically independent samples. **k**, Cell viability (%) of MB436 cells stably expressing shRNA-resistant BACH1(WT), BACH1(mut) or shCont vectors treated with vehicle, hemin (20 μM) or metformin (5 mM) for 48 h. Representative western blots of BACH1 expression are shown. Each experiment was repeated independently three times with similar results. For growth and viability assays in **a**, **d**, **e**, **i**, **j** and **k**, data are mean ± s.e.m., $n = 4$ biologically independent samples), unpaired two-tailed *t*-test.

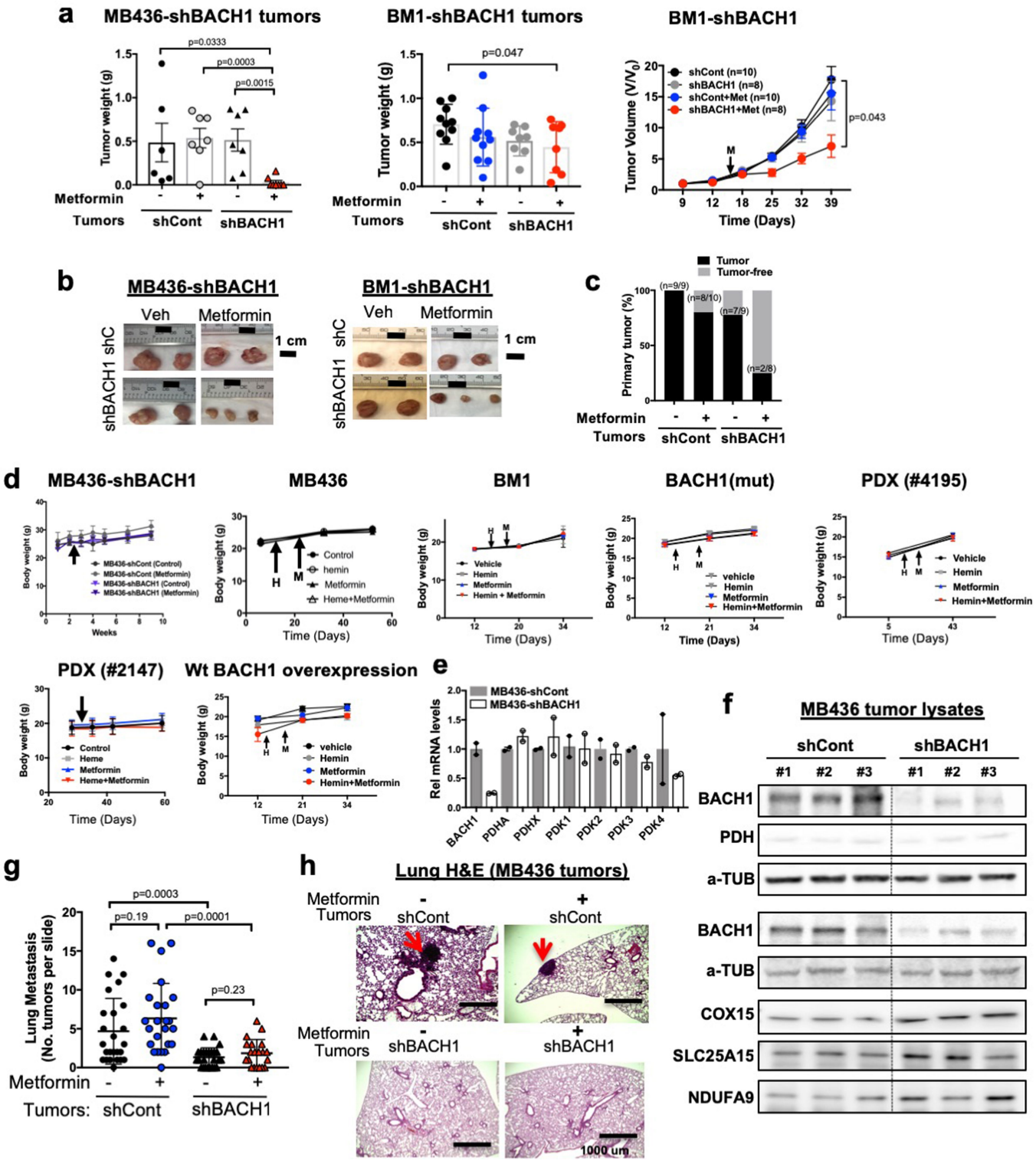

Extended Data Fig. 6 | Metformin suppresses growth of BACH1-depleted breast tumours. a, Tumour weights and volumes of mice injected with MB436-shBACH1 or control cells (left, $n = 6–7$ per group) or BM1-shBACH1 or control cells (right, $n = 8–10$ per group) and treated with vehicle or metformin. Data are mean ± s.e.m., unpaired two-tailed *t*-test. **b**, Tumour images of representative mice in each treatment group of mouse models. Scale bar, 1 cm. **c**, Primary tumour (%) indicates the ratio of mice with tumours or tumour-free upon metformin treatment compared to the total number of mice per treatment group at the end of experiment. **d**, Body weights of mice monitored before and after treatment of hemin and metformin. Arrow indicates initiation of hemin (H) or metformin (M) treatment. **e**, Relative mRNA expression of PDK and PDH mRNAs in tumours from MB436-shBACH1 xenograft mice by qRT–PCR. Data are mean ± s.e.m., $n = 2$ per group. **f**, Representative western blots of total PDH, BACH1 and mitochondrial membrane proteins (COX15, SLC25A15, NDUFA9) using MB436-shBACH1 or control tumour lysates. Each experiment was repeated independently three times with similar results. **g**, Lung metastases from mice with MB436-shBACH1 or control xenograft tumours. Lung tissues sectioned and H & E-stained to visualize and count lung metastases in mice. $n = 5$ mice per group. Data are mean ± s.e.m., two-tailed unpaired *t*-test. **h**, Representative lung metastasis images. Arrow indicates tumour metastases with a scale bar (1000 μm).

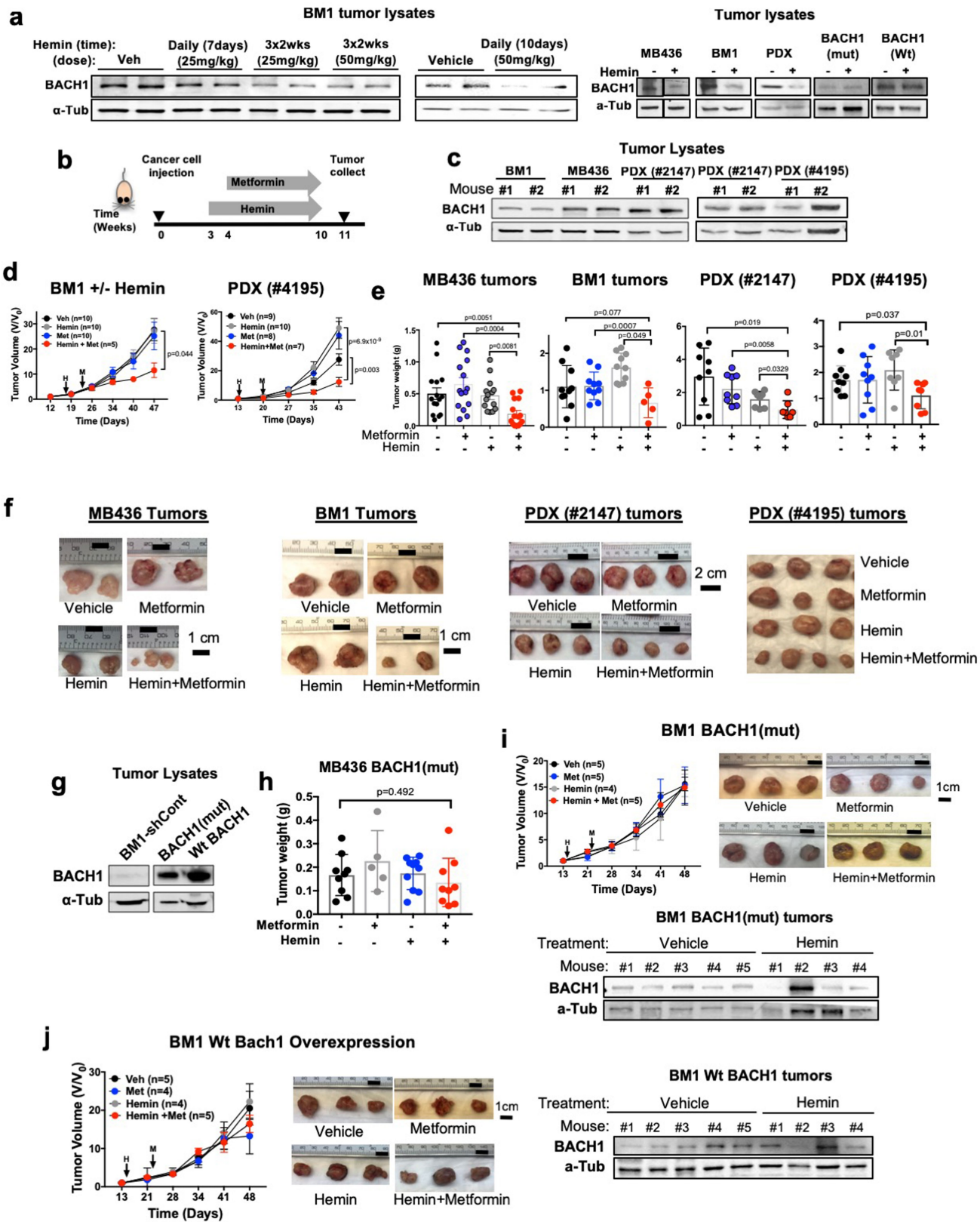

Extended Data Fig. 7 | See next page for caption.

Extended Data Fig. 7 | Combination treatment using hemin and metformin suppresses growth of tumours through BACH1 in multiple TNBC mouse models. a, Left, monitoring of BACH1 degradation by hemin treatment assayed by western blotting using tumour lysates. Mice ($n = 2$ per treatment group) injected with BM1 cells (2×10^6 cells) for 4 weeks to form tumours were treated with 25 mg kg^{-1} or 50 mg kg^{-1} hemin for the indicated times. Right, representative western blots showing relative BACH1 expression using tumours from mice treated with hemin for the experiments (see Fig. 4a–d). Western blotting experiments were repeated at least twice with similar results. **b**, Schematic depicting experimental plans with time line for cancer cell injection, hemin treatment (50 mg kg^{-1} day^{-1}) or metformin treatment (200–300 mg kg^{-1} day^{-1}) using TNBC mouse models. **c**, Representative western blots showing relative BACH1 expression from xenograft tumour models using tumours derived from BM1 cells, MB436 cells or two independent patients ($n = 2$ biologically independent samples). Western blotting experiments were repeated twice with similar results. **d**, Relative tumour volumes of BM1 or PDX (no. 4195) mouse xenograft monitored weekly during treated with vehicle, hemin or metformin. Tumour volume data are mean ± s.e.m., two-way ANOVA with multiple comparisons. BM1 tumours (vehicle $n = 10$, hemin $n = 10$, metformin $n = 10$, hemin + metformin $n = 5$) or PDX tumours (vehicle $n = 9$, hemin $n = 10$, metformin $n = 8$, hemin + metformin $n = 7$). **e**, Tumour weights, collected and measured at the end of the treatment using hemin and metformin of MB436, BM1-xenograft, or two PDX models (no. 2147 and no. 4195). Data are mean ± s.e.m. with *P* values using unpaired two-tailed *t*-test. **f**, Representative tumour images from each treatment group of MB436, BM1-xenograft or two PDX models are shown. Scale bar. 1 cm. **g**, Representative western blots of BACH1 using tumour lysates from mice xenografted with BM1-shCont, BM1-shBACH1 expressing BACH1(mut) or BM1-shBACH1 expressing wild-type BACH1. **h**, Tumour weights from mice xenografted with MB436-shBACH1 cells expressing BACH1(mut) and treated with vehicle, hemin or metformin. Data are mean ± s.e.m., two-tailed *t*-test. **i**, **j**, Tumour growth of BM1 BACH1(mut) (vehicle $n = 5$, hemin $n = 4$, metformin $n = 5$, hemin + metformin $n = 5$) or wild-type BACH1 xenografts (vehicle $n = 5$, hemin $n = 4$, metformin $n = 4$, hemin + metformin $n = 5$) treated with vehicle or hemin and representative tumour images from each treatment group of mice. Scale bar, 1 cm. Representative western blots showing BACH1 expression in multiple mouse tumour lysates.

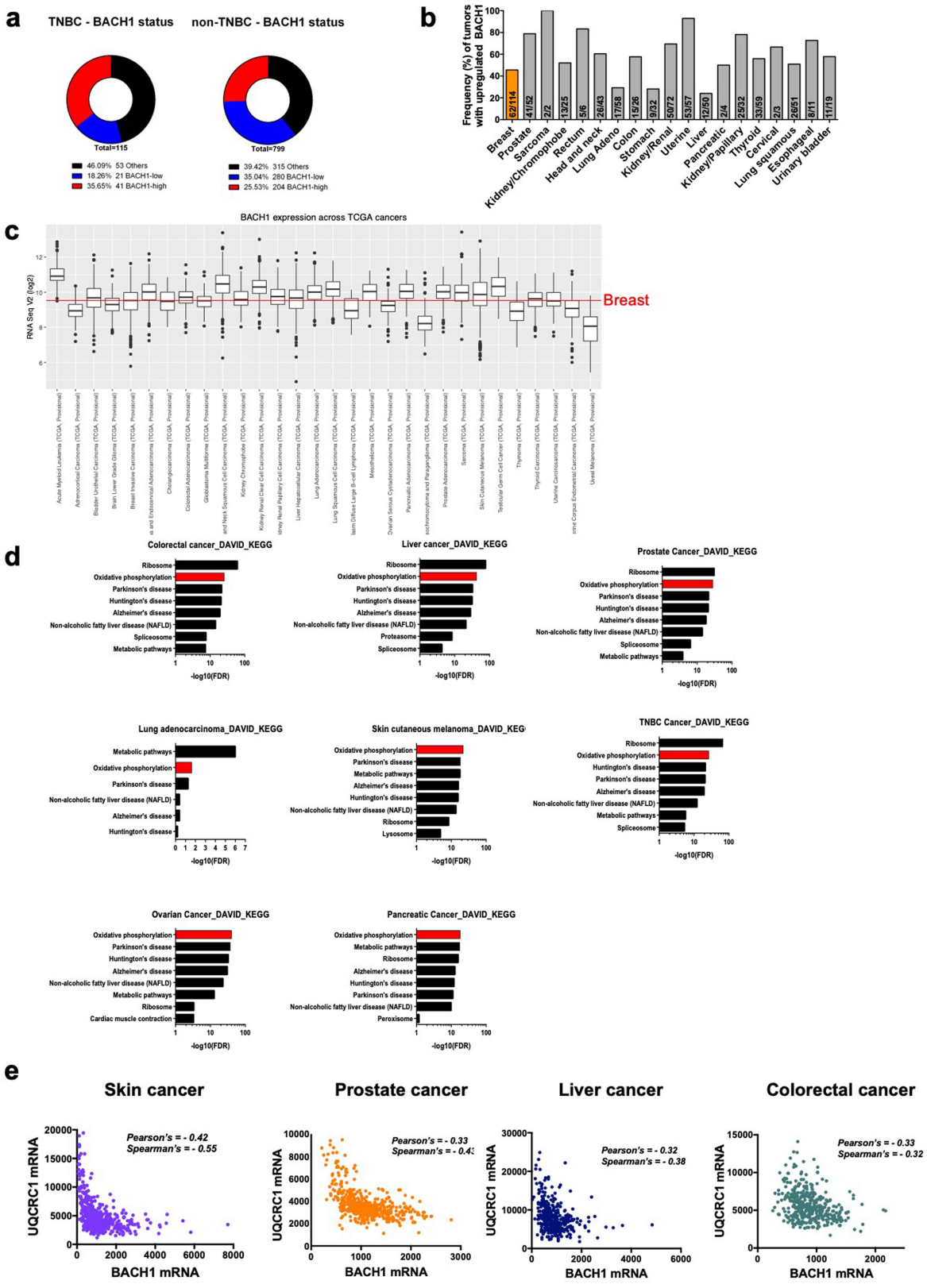

Extended Data Fig. 8 | See next page for caption.

Extended Data Fig. 8 | BACH1 expression in multiple cancer types. **a**, Distribution of BACH1 expression in TNBC. Clinical and RNA-seq data associated with the TCGA cohort of patients with breast cancer were accessed at https://www.cbioportal.org/. Out of all provisional cases ($n = 1{,}105$), breast cancer samples ($n = 914$) that had clinical information regarding receptor status of *ER*, *PR* (also known as *PGR*) and *HER2* (also known as *ERBB2*) based on immunohistochemistry analysis as well as RNA-seq data for BACH1-related genes were analysed. The TNBC subgroup among these 914 samples were identified as samples that are negative for all three receptors ($n = 115$). If the immunohistochemistry results were positive, indeterminate or equivocal for any of the three receptors, those samples were grouped in non-TNBC ($n = 799$). BACH1 status of the samples were based on an arbitrary 0.5 cut-off for the *z*-score transformed RNA-seq expression values for the *BACH1* gene (245 BACH1-high cases with *z*-score >0.5; 301 BACH1-low cases with *z*-score <0.5). **b**, Frequency (%) of patient tumours with overexpression of BACH1 compared to their matched normal tissues across multiple TCGA cancer types. Numbers of patients relative to healthy controls are indicated in the plot. **c**, Enriched BACH1 expression (RNA-seq) in TCGA provisional cancer datasets. Red bar indicates median BACH1 expression level in breast cancers. **d**, Extended plots from KEGG pathway analyses in Fig. 4f, carried out using DAVID using Benjamini-corrected *P* values (FDR), of genes that are negatively correlated with BACH1 expression. The top eight most-significantly enriched pathways with FDR values ($-\log(\text{FDR})$) are shown for each cancer type: colorectal, liver, lung, skin, ovary, pancreas, prostate and TNBC. **e**, Co-expression plots of *UQCRC1* and *BACH1* in TCGA cancers such as prostate ($n = 497$), skin ($n = 472$), liver ($n = 371$) and colon ($n = 379$). Pearson's (<-0.3) and Spearman's (<-0.3) correlation coefficients are shown.

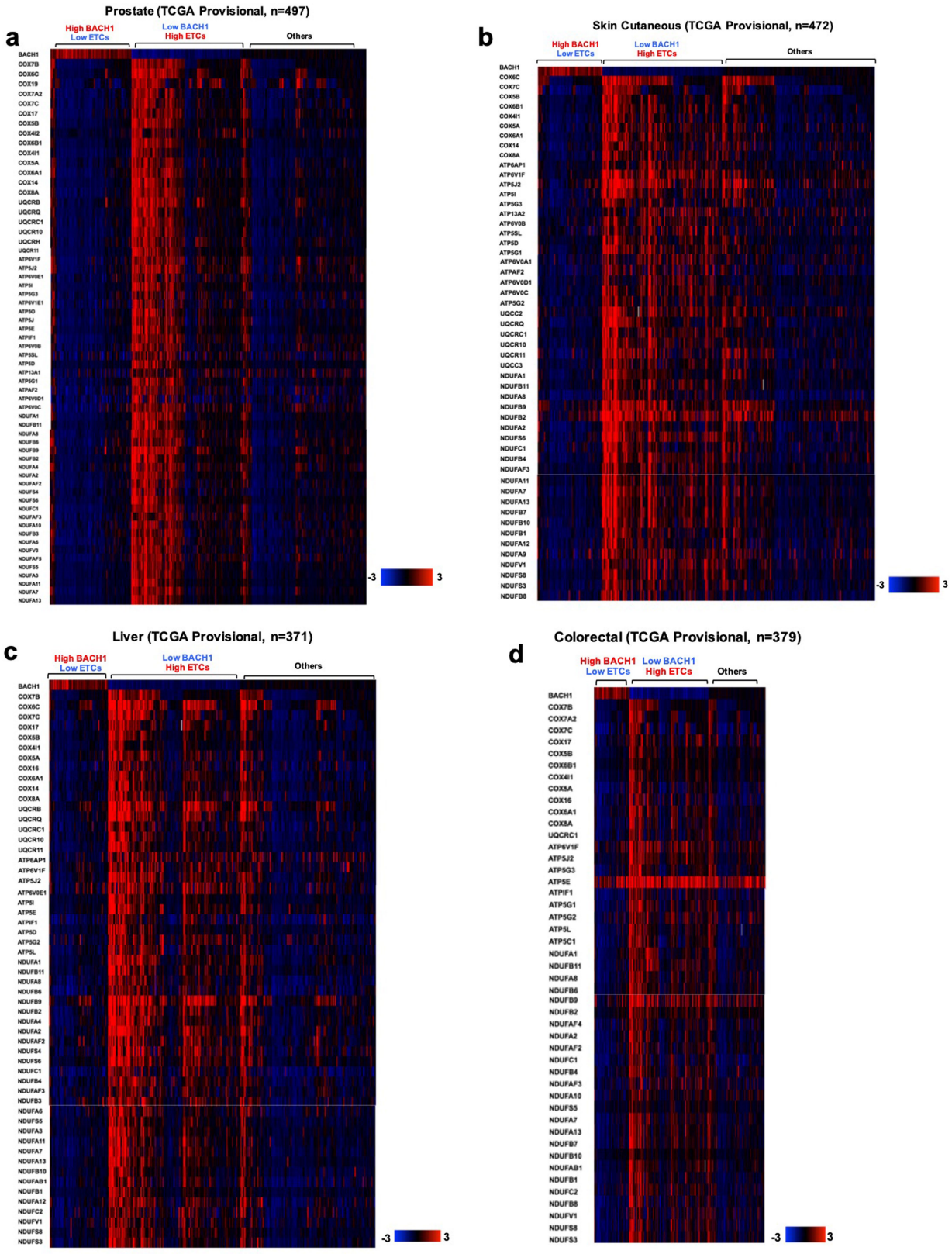

Extended Data Fig. 9 | OncoPrint analyses of multiple cancer types. **a**–**d**, Heat maps demonstrating upregulation (red) or downregulation (blue) of BACH1 and ETC genes across TCGA tumours (**a**, prostate carcinoma TCGA provisional, $n = 497$; **b**, patients with skin cutaneous cancer TCGA provisional, $n = 472$; **c**, patients with liver cancer TCGA provisional, $n = 371$; **d**, patients with colorectal cancer TCGA provisional, $n = 379$).

Extended Data Table 1 | List of primers for gene expression analysis using qRT–PCR and ChIP assays

Primers for Real Time RT-PCR		
Genes	Forward primer (5′-3′)	Reverse primer (3′-5′)
BACH1	CACCGAAGGAGACAGTGAATCC	GCTGTTCTGGAGTAAGCTTGTGC
ATP5J	GTTCTCCTCTGTCATTCGGTCA	TCCAGATGTCTGTCGCTTAGAT
ATP5G	CCAGAGTTGCATACAGACCAAT	CCCATTAAATACCGTAGAGCCCT
ATP5D	TCCCACGCAGGTGTTCTTC	GGAACCGCTGCTCACAAAGT
COX15	CAGCGCCTAGAGCACAGTG	GCCAGACTCTGTCAACCTAGT
COX18	GGGCAGCATTCTGCTCTCC	CCCAACTGATTTGCACGAACT
HSD3B	CACATGGCCCGCTCCATAC	GTGCCGCCGTTTTTCAGATTC
MRPL10	CACCGTCGTGTGATGCACTT	CGGCTATCATTCGGTTGTCCT
NDUFA9	GTCACGTTCTGCCATTACTGC	GGTGGTTGACAACATATCGCC
NDUFB6	CCACAGAAGATGGGGCCTATG	TCCAGACAGGTACAAGTACATGA
NDUFS7	CTTCGCAAGGTCTACGACCAG	GGAATAGTGGTAGTAGCCTCCTC
OCT1	GTG TGT AGA CCC CCT GGC TA	GTG TAG CCA GCC ATC CAG TT
PDHA	TGGTAGCATCCCGTAATTTTGC	ATTCGGCGTACAGTCTGCATC
PDHB	AAGAGGCGCTTTCACTGGAC	ACTAACCTTGTATGCCCCATCA
PDHX	TTGGGAGGTTCCGACCTGT	CAACCACTCGACTGTCACTTG
SLC25A15	CCTGAAGACTTACTCCCAGGT	GCGATGTTGGCGATTAGTGC
SLC25A22	GCCAGCCAAGCTCATCAATG	GAGGCAGTCGGACATGCTC
TIMM17A	GGTGGGGCCTTTACGATGG	GCCCTGGTTTTAATAGCTGTCA
TIMM8B	TCACTTCATGGAGTTATGTTGGG	AGACAATTTTCAGTGCGAGAGTC
UCP3	TGTTTTGCTGACCTCGTTACC	GACGGAGTCATAGAGGCCGAT
UQCRC1	GGGGCACAAGTGCTATTGC	GTTGTCCAGCAGGCTAACC
Primers for ChIP assays		
ATP5D	GAGGAAGCCTGGTCAGCTC	CAGGGAAGACCCAGCTTGT
ATP5J	AACTGGAGTCCCAAAAGGCC	GAAGTAGAGCGGAGGTGGTG
COX15	TGGGACAGGGATGAGTGATT	TGTCTGCTTTGTTTTCATTTGC
COX18	ACTGTTGATGACTGAAAAGCCA	AAAAGCCACCACTGTTCCCA
SLC25A22	GCCAGGTCGATGGGAAACA	CATGGTCAAGGAAGCCGGT
TIMM8B	AGCCCATACCTCTGTAGCCA	CCCGTGCTGAACAAGAGTCA
UCP3	AAAGCTCTGCCTAAGACCGC	CCATCCAGGAGCGACAGAAA
UQCRC1	GTTGGGATGGAGGTTGAATGA	GTGTGTATCTCTGTGCCTGTG
PDK1	AACAAGGGCAGCTTGGAAGT/	GTGAGGGGGTGAGTCAGTTC
PDK2	TGCACACAAGGGACCTTCAG	TCGACCTTGGGAGGAAATGC
PDK3	ACACAAACGTCACAGAGGCA	GAGTCGGTTGCTGCACGTA
PDK4	GGCTTGGGTTTCCTGTCTGT	AGCGGGTCACATTCTCAGTG

Corresponding author(s): Marsha Rich Rosner (mrosner@uchicago.edu)

Reporting Summary

Nature Research wishes to improve the reproducibility of the work that we publish. This form provides structure for consistency and transparency in reporting. For further information on Nature Research policies, see Authors & Referees and the Editorial Policy Checklist.

Statistical parameters

When statistical analyses are reported, confirm that the following items are present in the relevant location (e.g. figure legend, table legend, main text, or Methods section).

n/a	Confirmed	
☐	☒	The exact sample size (*n*) for each experimental group/condition, given as a discrete number and unit of measurement
☐	☒	An indication of whether measurements were taken from distinct samples or whether the same sample was measured repeatedly
☐	☒	The statistical test(s) used AND whether they are one- or two-sided *Only common tests should be described solely by name; describe more complex techniques in the Methods section.*
☐	☒	A description of all covariates tested
☐	☒	A description of any assumptions or corrections, such as tests of normality and adjustment for multiple comparisons
☐	☒	A full description of the statistics including central tendency (e.g. means) or other basic estimates (e.g. regression coefficient) AND variation (e.g. standard deviation) or associated estimates of uncertainty (e.g. confidence intervals)
☐	☒	For null hypothesis testing, the test statistic (e.g. *F*, *t*, *r*) with confidence intervals, effect sizes, degrees of freedom and *P* value noted *Give P values as exact values whenever suitable.*
☒	☐	For Bayesian analysis, information on the choice of priors and Markov chain Monte Carlo settings
☒	☐	For hierarchical and complex designs, identification of the appropriate level for tests and full reporting of outcomes
☒	☐	Estimates of effect sizes (e.g. Cohen's *d*, Pearson's *r*), indicating how they were calculated
☐	☒	Clearly defined error bars *State explicitly what error bars represent (e.g. SD, SE, CI)*

Our web collection on statistics for biologists may be useful.

Software and code

Policy information about availability of computer code

Data collection	No specific software was used for data collection.
Data analysis	GraphPad PRISM 7.0 and Microsoft Excel were used for statistical data analysis.

For manuscripts utilizing custom algorithms or software that are central to the research but not yet described in published literature, software must be made available to editors/reviewers upon request. We strongly encourage code deposition in a community repository (e.g. GitHub). See the Nature Research guidelines for submitting code & software for further information.

Data

Policy information about availability of data

All manuscripts must include a data availability statement. This statement should provide the following information, where applicable:

- Accession codes, unique identifiers, or web links for publicly available datasets
- A list of figures that have associated raw data
- A description of any restrictions on data availability

All data are available from the authors upon reasonable request.

Field-specific reporting

Please select the best fit for your research. If you are not sure, read the appropriate sections before making your selection.

☒ Life sciences ☐ Behavioural & social sciences ☐ Ecological, evolutionary & environmental sciences

For a reference copy of the document with all sections, see nature.com/authors/policies/ReportingSummary-flat.pdf

Life sciences study design

All studies must disclose on these points even when the disclosure is negative.

Sample size	No statistical methods were used to predetermine sample size.
Data exclusions	No data are excluded for analysis.
Replication	All experiment (except metabolic tracing and metabolic profiling, which were done once) were repeated at least 3 times with similar results. Both technical and biological replicates were reliably reproduced.
Randomization	For animal experiments, mice were randomized before treatment and allocated for treatment to avoid cage or tumor injection order effect. The other experiments were not randomized.
Blinding	The experiments were not blinded.

Reporting for specific materials, systems and methods

Materials & experimental systems

n/a	Involved in the study
☒	☐ Unique biological materials
☐	☒ Antibodies
☐	☒ Eukaryotic cell lines
☒	☐ Palaeontology
☐	☒ Animals and other organisms
☒	☐ Human research participants

Methods

n/a	Involved in the study
☒	☐ ChIP-seq
☒	☐ Flow cytometry
☒	☐ MRI-based neuroimaging

Antibodies

Antibodies used	BACH1 (Santa Cruz, sc-271211, Lot #E1418, 1:1000), PDK1 (C47H1) (Cell Signaling, #3820, Lot#12, 1:500), PDH (Cell Signaling, #2784, Lot#2, 1:1000), PDH [p-Ser293] (Novusbio, BB110-93479, Lot#0-1, 1:1000), ATP5D (Abcam, ab107077, Lot#GR75494-3, 1:500), SLC25A15 (Novusbio, NBP2-20387, Lot#40366, 1:500), UQCRC1 (Abcam, ab118687, Lot#GR164879-7, 1:500), COX15 (Sigma, av46442-100UL, Lot# QC16365, 1:1000), NDUFA9 (Abcam, ab14713, LOT#GR289427-3), and alpha-Tubulin (Santa Cruz, sc-8035, Lot#K0816, 1:5000) for western blotting. For secondary antibodies for western, IRDye 800CW Goat anti-Mouse IgM (929-32280, Lot# C80402-15, 1:5000), IRDye 680RD Goat anti-Rabbit (Li-Cor, 926-68071, Lot#C80426-05, 1:5000), IRDye 800CW Goat anti-Mouse (Li-Cor, 926-32210, Lot#C80306-02, 1:5000), IRDye 680RD Goat anti-Mouse (Li-Cor, 926-68070, Lot#C70908-04, 1:5000), Anti-mouse IgG-HRP (Sigma, A4416-1ML, Lot#041M6237, 1:5000) and Anti-Rabbit IgG HRP (Millipore AP187P, Lot#2920422, 1:5000). BACH1 (AF5776, R&D System; Santa Cruz, sc-271211), RNA Pol II phosphoS5 (Abcam, ab5131), Mouse monoclonal to Histone H3 tri methyl K27-ChIP grade (Abcam, ab6002) and IgG (normal mouse/goat/rabbit IgG, Santa Cruz, sc-2025/sc-3887/sc-2027) for ChIP assays.
Validation	Each antibody used in this work was validated for its use by manufacturers.

Eukaryotic cell lines

Policy information about cell lines

Cell line source(s)	Human breast cancer cell lines (MDA-MB-436, MDA-MB-468) and nonmalignant mammary epithelial cells (MCF10A and 184A1) were obtained from ATCC, and BM1 cells were obtained from Dr. Andy Minn's laboratory (University of Pennsylvania)
Authentication	Cell line authentification was validated by STR analysis.

Mycoplasma contamination	Mycoplasma detection was routinely performed to ensure cells are not infected with mycoplasma using MycoAlert Detection kit (Lonza, LT07-218).
Commonly misidentified lines (See ICLAC register)	N/A

Animals and other organisms

Policy information about studies involving animals; ARRIVE guidelines recommended for reporting animal research

Laboratory animals	Athymic nude and SCID BEIGE female mice with age of 4-6 weeks to generate xenograft tumors were purchased from Charles River Laboratory.
Wild animals	This study did not involve wild animals.
Field-collected samples	This study did not involve samples collected from the field.